The Structure of a Subtropical Prefrontal Convective Rainband. Part I: Mesoscale Kinematic Structure Determined from Dual-Doppler Measurements

YEONG-JER LIN

Department of Earth and Atmospheric Sciences, Saint Louis University, St. Louis, Missouri

ROBERT W. PASKEN

Department of Science and Mathematics, Parks College of Saint Louis University, Cahokia, Illinois

HSIU-WU CHANG

Department of Earth and Atmospheric Sciences, Saint Louis University, St. Louis, Missouri

(Manuscript received 23 July 1991, in final form 10 January 1992)

ABSTRACT

In Part I of this study, structural features of a convective rainband associated with the Mei-Yu front on 25 June 1987 over northwestern Taiwan are investigated. The dynamic and thermodynamic structures and momentum budgets of the convective rainband will be reported in Part II. Dual-Doppler data were collected from CP-4 and TOGA Doppler radars positioned along the northwest coast of Taiwan during the Taiwan Area Mesoscale Experiment (TAMEX). Fields of the system-relative wind and reflectivity were derived in a horizontal domain of 40 km × 36 km using the objective analysis scheme with a 1-km grid spacing in all three directions. There were ten analysis levels in the vertical ranging from 0.8 to 9.8 km. Vertical velocities were computed from the anelastic continuity equation by integrating downward with variational adjustment.

Results show that the low-level jet (LLJ) in the boundary layer provides large vertical shear ahead of the cold front. The orientation of the jet is in the direction almost parallel to the cold front. The depth of the cold air associated with the Mei-Yu front is rather shallow (1–2 km), in agreement with other TAMEX case studies reported in the literature. To the south of the front, winds are from the southwest in the lower troposphere and veer with height in the middle and upper troposphere. The southwest monsoon flow at low levels transports high-θ_e environmental air toward the wind-shift line. Behind the front, the northwesterly flow dominates, carrying much cooler air from northern China. The low-level convergence enhances lifting, resulting in a narrow band of convection on the warm side of the front. The length of the rainband analyzed is 5–10 km wide and 50 km long and is composed of many cells. Each cell is accompanied by the moderate convective updraft (6–8 m s^{-1}) and weak downdraft (2–4 m s^{-1}). The precipitation is deep but not intense on the warm side of the front. The maximum reflectivity within the rainband is less than 42 dBZ. The precipitation cores are elongated southeastward in the direction parallel to the environmental shear vector between the lower and middle layers. By contrast, the precipitation behind the front is weak and shallow, showing stratiform precipitation. Because the system traveled very slowly within the domain of interest, up to 200 mm of rainfall in 24 h occurred on the west coast of central Taiwan.

1. Introduction

Structural features of narrow frontal rainbands in the midlatitudes were reported in studies by Browning and Harrold (1970), Browning and Pardoe (1973), Houze et al. (1976), Matejka et al. (1980), Hobbs and Persson (1982), Carbone (1982, 1983), Parsons et al. (1987), Lemaitre et al. (1989), etc. Carbone (1982) studied a severe frontal rainband in the Central Valley of California using triple-Doppler radar data. The structure of this rainband resembled that studied by Browning and Harrold (1970). Intense planetary boundary layer (PBL) forcing of a low-level jet (LLJ) by the gravity–density current propagation mechanism was responsible for producing a two-dimensional prefrontal updraft of 15–20 m s^{-1} with a maximum occurring at 2.1 km above ground level (AGL). In a related study, Parsons et al. (1987) investigated the thermodynamic structure of the same frontal rainband studied by Carbone (1982) using the thermodynamic retrieval method of Gal-Chen (1978). They found that the dynamics of the front were similar to a density current. The updraft at the leading edge of the cold air mass was probably maintained by an upward pressure gradient force. The kinematic structure of a cold-frontal rainband over southwestern France was studied by Le-

Corresponding author address: Dr. Yeong-Jer Lin, St. Louis University, Department of Earth and Atmospheric Sciences, 3507 Laclede Avenue, St. Louis, MO 63103.

maitre et al. (1989) using dual-Doppler data. Results showed that a rainband was oriented along the surface front and was nearly perpendicular to the vertical shear of the environmental wind with high-reflectivity cores elongated in the direction of the environmental shear vector. In the convective region, the low-level cold flow acted as a gravity current by lifting the PBL air upward and inducing new cells ahead of the system.

Observational evidence reveals that the organized mesoscale convective systems (MCSs) are often embedded within a broad Mei-Yu cloud band on the warm side of the front. These convective systems move from the west to east in a direction almost parallel to the front. As the MCSs approach Taiwan, they frequently interact with the central mountain range (CMR), resulting in locally heavy rainfall. The major objectives of TAMEX (Taiwan Area Mesoscale Experiment) were to study 1) the mesoscale circulation of the Mei-Yu front; 2) MCSs within the Mei-Yu frontal zone; and 3) the effects of topography on the Mei-Yu front and precipitation processes (Kuo and Chen 1990). During the TAMEX field project, three 5-cm Doppler radars were positioned along the northwest coast of Taiwan (Fig. 1), including the NCAR (National Center for Atmospheric Research) CP-4, TOGA (Tropical Ocean Global Atmosphere), and CAA (Civil Aeronautic Administration) radars.

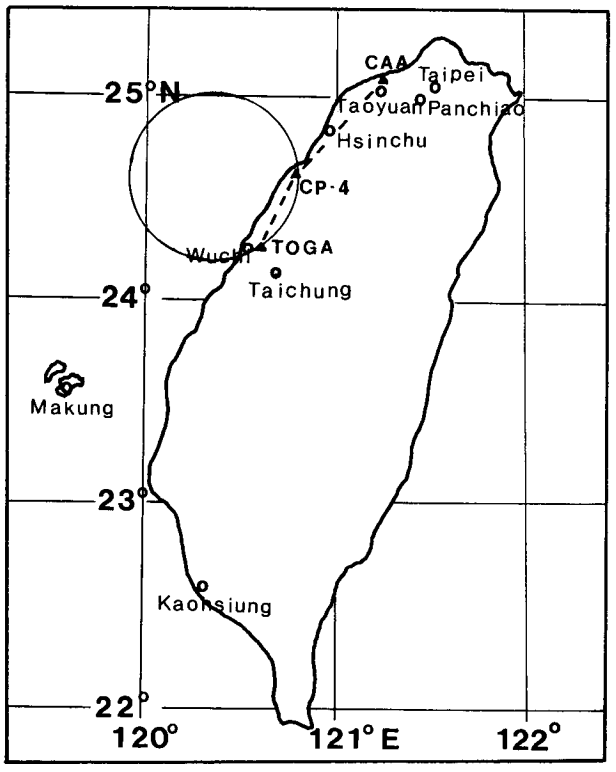

FIG. 1. A TAMEX Doppler network showing locations of the CP-4, TOGA, and CAA radars. A circle signifies the dual-Doppler coverage area of CP-4 and TOGA.

The effects of the CMR on the Mei-Yu front and rainfall distribution over the island of Taiwan during TAMEX intensive observing period 13 (IOP 13) were investigated in the study by Mannouji and Kurihara (1990) using the spectral limited-area model of JMA (Japan Meteorological Agency). Two experiments were conducted using the enhanced TAMEX data as the initial condition: one with the CMR and the other without the CMR. Results showed that the presence of the CMR causes 1) the position of the precipitation area and wind convergence zone to be shifted; 2) the rainfall amount to be increased by 2–3 times compared to that of no mountain; 3) the surface wind-shear line to be discontinuous across the island of Taiwan; and 4) the mesolow to occur to the southeast of Taiwan.

The purpose of this study is to investigate some mesoscale structural features of a convective rainband in the subtropical region associated with the Mei-Yu front on 25 June during TAMEX IOP 13. Part I emphasizes the kinematic structure of the rainband using dual-Doppler–derived winds and surface and upper-air observations. The dynamic and thermodynamic properties and momentum budgets of the rainband will be presented in Part II. In Part I, the environmental conditions conducive to development of this MCS are presented. Additionally, the environmental conditions after the passage of the front are also analyzed to illustrate the effect of convection on its immediate environment. Results obtained are then compared to other cases in TAMEX and elsewhere. The goal is to gain a better understanding of the mesoscale structure of a Mei-Yu prefrontal convective system that produced heavy precipitation in northwestern and central Taiwan.

The weather conditions, radar signatures, and surface parameters are detailed in section 2. Section 3 describes the environmental wind shear and stability conditions prior to and after the passage of the Mei-Yu front. Data analysis and computational procedures are presented in section 4. Results are discussed in section 5, followed by the conclusions in section 6.

2. Weather situation and surface parameters

a. Synoptic condition

The satellite IR image for 1500 UTC 24 June is shown in Fig. 2. At the time of observation, the Mei-Yu front was located over the northern tip of Taiwan. In the Taiwan Strait, a narrow cloud band was visible in conjunction with convective activity near the cold front.

The IOP 13 started at 1400 UTC 24 June. At this time the upper-air sounding network began collecting 3-h data and the conventional surface network started taking high-frequency (30-min) observations.

The upper-air charts of 1200 UTC 24 June are presented in Fig. 3. At 850 mb (Fig. 3a), a low pressure system was just southwest of Japan. A temperature trough (heavy dashed line) extended southwestward

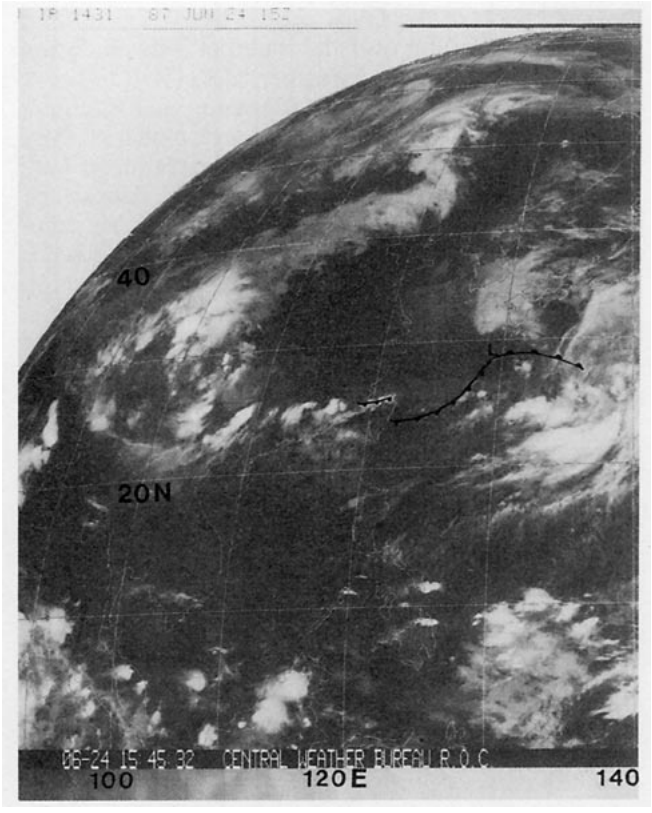

FIG. 2. An IR satellite image at 1500 UTC 24 June 1987. The approximate position of the front is superimposed.

from the low center into the western part of the Taiwan Strait with strong horizontal shear just to the west. The southwest monsoon flow prevailed over the strait and its vicinity, carrying moisture-rich air from the warmer region to the south into the area. This air was conditionally unstable and favorable for MCS development (Kuo and Chen 1990; Jou and Deng 1990; etc.).

At 700 mb (Fig. 3b), the winds became westerly at 10–13 m s^{-1} over the strait. In the midtroposphere (Fig. 3c), the winds were from the northwest and reduced in speed to about 10 m s^{-1}. At 200 mb (Fig. 3d), the winds shifted to the north, increasing in speed to 15 m s^{-1}. An area of diffluence occurred over northern Taiwan and its vicinity. The dominance of diffluence in the upper troposphere with large-scale confluence at low levels contributed to unstable environmental conditions in the warm sector favorable for thunderstorm development (see Jou and Deng 1990; Lin et al. 1990 for details).

The successive positions of the Mei-Yu front at the surface from 0000 UTC 24 June to 0600 UTC 25 June, in intervals of 3 h, during IOP 13 were analyzed by Jou and Deng (1990) using the enhanced surface data. Figure 4 is reproduced from their study. It reveals that the Mei-Yu front passed through Taiwan between 0900 UTC 24 June and 0000 UTC 25 June. Due to the effect of the CMR, the eastern part over the Pacific Ocean continues to travel at a rapid speed toward the southeast, while the western part (west and southwest of Taiwan) often remains quasi-stationary. The jump between 0900 and 1200 UTC was properly caused by the increase in water temperature over the Pacific Ocean.

b. *Radar signatures*

As described in the radar summary of IOP 13 (Parsons and Trier 1989), an active convective line with reflectivity greater than 50 dBZ occurred to the northwest of Taiwan in the early morning hours of 25 June. The convective activity associated with the Mei-Yu front continued as it approached the west coast of Taiwan. The radar analysis of this convective rainband was reported in the study by Lin et al. (1990) using both single- and dual-Doppler data.

The PPI (plan position indicator) displays as seen from the conventional 10-cm radar in Kaohsiung from 0400 to 1100 LST 25 June are depicted in Fig. 5. The approximate positions of the Mei-Yu front as depicted in Fig. 4 are superimposed. Notice that a line of convection oriented in an east-northeast–west-southwest direction parallel to the front developed in a broad area ahead of the Mei-Yu front described earlier. This prefrontal rainband traveled at a very slow speed toward the south. As the system entered the dual-Doppler coverage area of CP-4 and TOGA (see the circle in Fig. 1), it produced extremely heavy precipitation in the area near the TOGA radar site. Up to 200 mm of rainfall in 24 h occurred in that area.

c. *Surface observations*

The surface map at 1200 UTC (20 LST) 24 June is presented in Fig. 6a. Note that the eastern part of the front had already passed through northern Taiwan. However, the western portion of the front remained nearly stationary from the northern tip of Taiwan westward to the eastern China coast. In the vicinity of the front, cooler temperatures, low dewpoint depression, and precipitation were reported. Winds shifted from the north and northeast to south and southwest across the front. The front had features characteristic of a Mei-Yu front (Kuo and Chen 1990). At 0000 UTC (0800 LST) 25 June (Fig. 6b), the eastern part of the front was located over the southern tip of Taiwan, while the western portion moved very slowly toward the south at 2–3 m s^{-1}. Behind the front, the winds were from the northeast, transporting cooler air from the mainland of China to eastern and northwestern Taiwan. Conversely, the southwesterly flow dominated the regions ahead of the front. Continuous rainfall was reported along the front.

The surface observations at two northern stations (Taoyuan and Hsinchu, see Fig. 1) are shown in

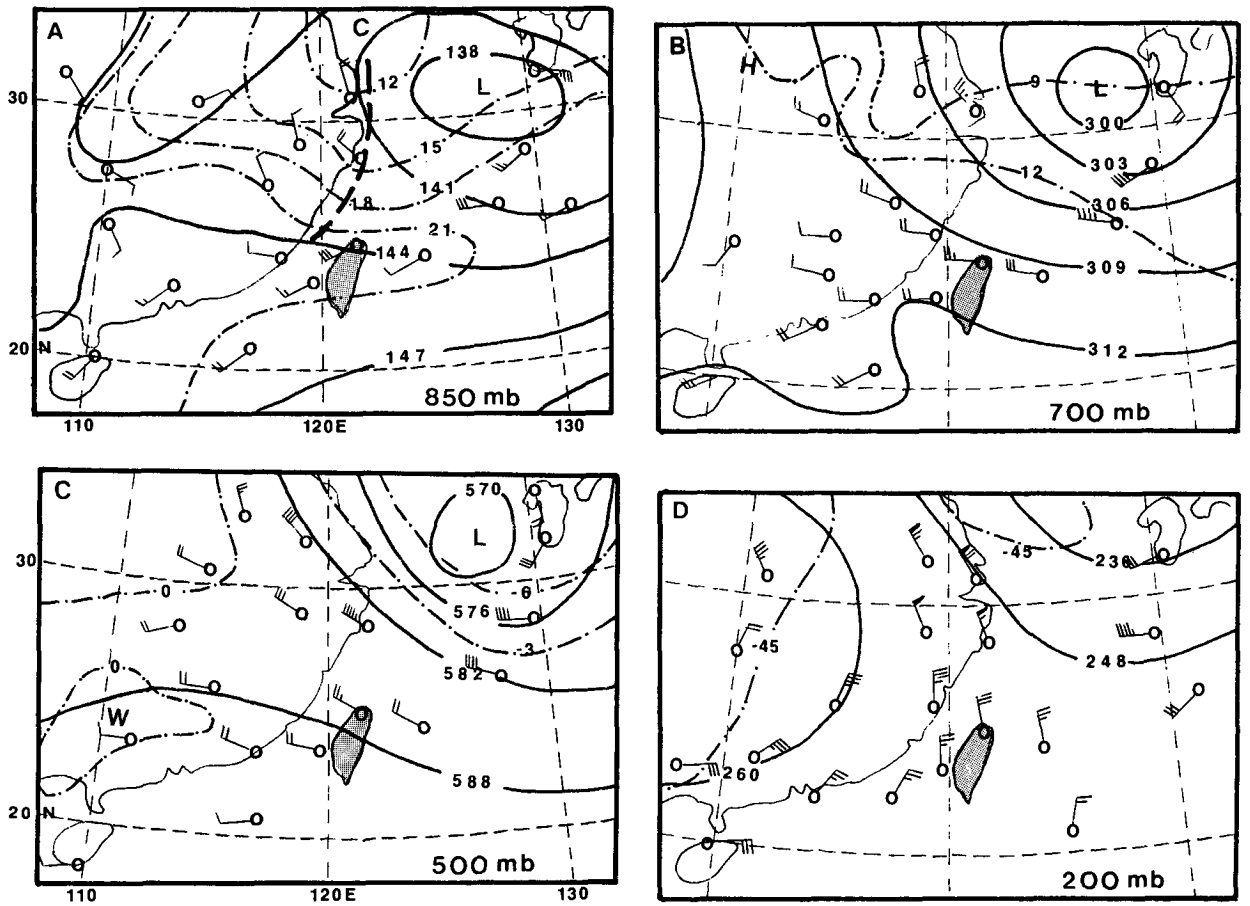

FIG. 3. Upper-air charts at 1200 UTC 24 June 1987, showing the large-scale airflow at (a) 850, (b) 700, (c) 500, and (d) 200 mb. Contour intervals for 850, 700, 500, and 200 mb are 30, 30, 60, and 120 m, respectively. Heavy solid and dash–dot lines represent the isopleths for height and temperature, respectively. The island of Taiwan is shaded.

Fig. 7. The vertical dashed line indicates the time of frontal passage. The Mei-Yu front passed through Taoyuan around 0400–0500 LST 25 June (Fig. 7a). At the time of frontal passage, the wind increased, gusting to 10 m s^{-1}, and changed its direction from the southwest to northeast. After frontal passage, the surface pressure rose 2–3 mb in a few hours and both the temperature T and dewpoint T_d decreased more than 5°C in 2 h. The temperature decrease was in part attributed to the arrival of cooler air from northern China. Examination of hourly temperature (solid) and dewpoint (dashed) curves reveals that the dewpoint depression was less than 2°C before frontal passage, indicative of high-θ_e air at low levels in the warm sector. The dewpoint depression reduced to nearly zero 1–4 h after frontal passage, showing cool, saturated air near the surface. Heavy precipitation (up to 30 mm h^{-1}), associated with the convective rainband, occurred 0–2 h before frontal passage. On the other hand, the dewpoint depression became larger 5–6 h after frontal passage, indicative of the dominance of low-θ_e air from northern China. This frontal system traveled slowly toward the south, reaching the Air Force Hsinchu station, approximately 40 km southwest of Taoyuan (Fig. 1), by 0730 LST. Figure 7b displays variations of the wind, pressure, temperature, dewpoint, and rainfall amount at Hsinchu. Similar to Taoyuan, the surface pressure rose and both temperature and dewpoint decreased considerably after frontal passage, except the magnitudes were somewhat smaller than those shown in Fig. 7a. Notice that heavy precipitation occurred 1–3 h before frontal arrival in association with the prefrontal convective rainbands.

The surface observations at CCK (Ching-Chung-Kang), where the TOGA radar was located, are presented in Fig. 8a. It shows that the front did not pass through the station until 2300 LST 25 June. This was also supported by the surface observations taken at Wuchi (not shown), located just west of TOGA (Fig. 1). It is seen that heavy precipitation occurred from 0800 to 1200 LST with a maximum of 50 mm h^{-1}. The dewpoint depression remained small (<1°C) throughout the day, due to the presence of high-θ_e air in the area. The changes in pressure and temperature

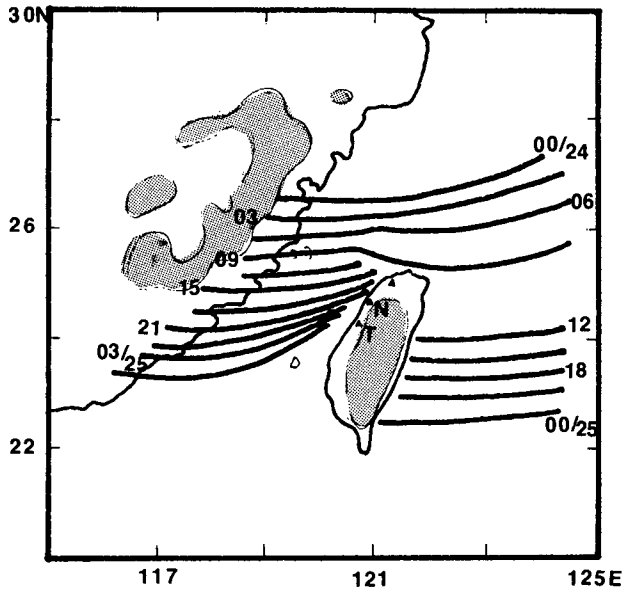

FIG. 4. The successive positions of the surface cold front from 0000 UTC 24 June to 0600 UTC 25 June 1987 in intervals of 3 h. The shaded area shows the heights of topography in excess of 600 m (after Jou and Deng 1990). The locations of CP-4 (N) and TOGA (T) are indicated.

after frontal passage were relatively small compared to those observed at Taoyuan and Hsinchu (Fig. 7).

Figure 8b shows the surface observations taken at Makung in the Taiwan Strait. This station is located about 250 km southwest of Taoyuan. The front passed through the station around 1900 LST 25 June. Unlike the features observed at two northern stations, variations of the surface pressure, temperature, and dewpoint at the times before and after frontal passage were quite small, due to the influence of warm oceanic waters in the strait. Trier et al. (1990) found that the postfrontal air mass on 8 June during TAMEX IOP 8 was substantially modified by heat fluxes over the Taiwan Strait as it moved southward over the warm oceanic waters. As a result, a 60%–70% decrease on the temperature contrast across the front was observed between ocean stations at the northern and southern ends of the island.

d. Rainfall distribution

As noted earlier, the portion of the Mei-Yu front west of Taiwan was moving very slowly from the northern tip of Taiwan toward south. The rainfall amount was recorded at higher-frequency rates (30 min) over most stations in the enhanced mesoscale network. The accumulated rainfall distribution from 0000 to 2400 LST 25 June over the island is presented in Fig. 9. Notice that up to 200 mm of rainfall in 24 h occurred in the areas northeast and southwest of Taichung (Fig. 1). Heavy precipitation was concentrated in most coastal areas west of the CMR and was

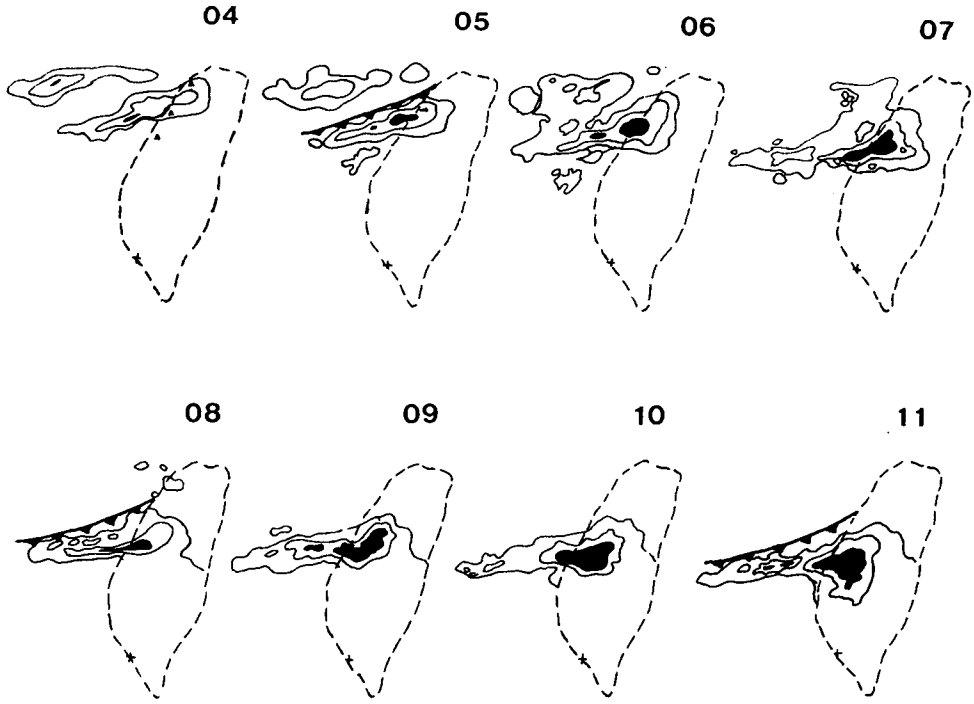

FIG. 5. The hourly PPI displays from 0400 to 1100 LST 25 June 1987 as seen from the 10-cm conventional Kaohsiung radar (+). Contour interval is 10 dBZ starting from 15 dBZ. The darkened area represents reflectivities greater than 35 dBZ. The positions of the cold front extracted from Fig. 4 are indicated.

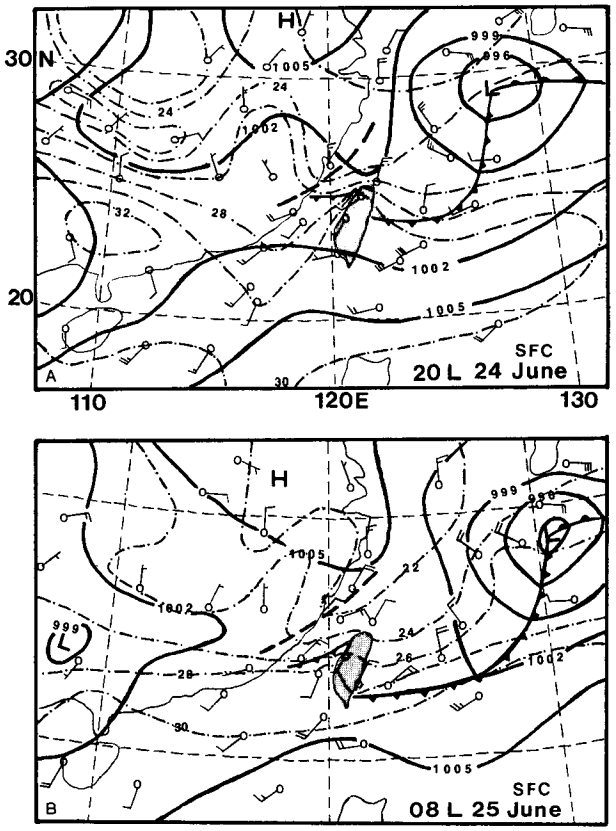

FIG. 6. Surface maps at (a) 2000 LST (1200 UTC) 24 June and (b) 0800 LST (0000 UTC) 25 June 1987. Heavy solid and dash-dot lines represent the isobars and isotherms, respectively. The island of Taiwan is shaded.

associated with the prefrontal convective rainband mentioned before.

3. Environmental wind shear and stability conditions

a. Upper-air characteristics

As stated earlier in section 1, the presence of a LLJ in the PBL plays an important role in enhancing low-level convergence for convective rainbands in the mid-latitudes (e.g., Browning and Harrold 1970; Carbone 1982; and many others). It is of interest to see the wind variability of large-scale flow before, during, and after the passage of a subtropical cold front.

Figure 10 displays time–height variations of the environmental winds based on rawinsonde observations at Makung and Panchiao. The Makung station is located in the Taiwan Strait where the influence of topography is of a minimum. By contrast, Panchiao is located over northern Taiwan near the city of Taipei (Fig. 1) and is surrounded by mountains with heights varying from 250 to 1000 m. At Makung (Fig. 10a), rawinsonde winds are plotted in intervals of every 3 h starting from 0200 LST and ending at 2300 LST 25 June. Recall that the cold front passed through the station by 1900 LST (see the arrow in Fig. 10). During the prefrontal period, the southwest monsoon flow prevailed in the lower troposphere. The LLJ with a maximum speed of 18 m s^{-1} was evident at the 930-mb level by 0500 LST. The direction of this jet was nearly parallel to the Mei-Yu front described earlier. Strong vertical wind shear occurred at levels above and below the LLJ. In the mid- and upper troposphere, however, no apparent mid- and upper-level jets were present. As the convective rainbands approached the station, a significant variation in wind speed took place at heights above 600 mb. By 1400 LST, the LLJ was no longer evident in the lower layer. Instead, a midlevel jet (MLJ) with maximum speeds in excess of 20 m s^{-1} developed in the layer between 350 and 500 mb. This time coincided with the convective activity at Makung. Approximately 20 mm of rainfall was reported at the station from 1300 to 1400 LST (see the vertical solid bar in Figs. 8b and 10a). Our momentum budget calculations (not shown) reveal that the development of this MLJ was largely caused by the vertical transport of horizontal momentum by convective eddies associated with the rainbands. The details will be reported in Part II.

Figure 10b depicts time–height variations of the environmental winds at Panchiao from 0800 LST 24 June to 1700 LST 25 June. The surface observations (not shown) indicate that the cold front passed through the station by 2300 LST 24 June, before the enhanced upper-air data were gathered. Prior to frontal passage, the LLJ with a maximum speed up to 25 m s^{-1} prevailed at the 900-mb level. This speed was stronger than that observed at Makung (Fig. 10a). Notice that the observational times of the LLJ at the two stations were different. Examination of Fig. 10b further reveals that no mid- and upper-level jets were visible before the convection in agreement with those shown in Fig. 10a. The LLJ was lifted to the 700–800-mb layer after 0200 LST 25 June. The convection continued from 0200 to 0800 LST [see the vertical solid bar, rainfall rate (mm h^{-1}), in Fig. 10b]. The MLJ formed at 500 mb during the convection with a maximum speed of 25 m s^{-1} by 0500 LST. This feature is similar to that observed at Makung (Fig. 10a). Both the MLJ and LLJ weakened substantially after the convection.

In an effort to illustrate the changes in atmospheric thermodynamics and stability from the prefrontal environment to the postfrontal environment, the time–height cross section of equivalent potential temperature θ_e for Panchiao is shown in Fig. 11. Moist static energy is proportional to θ_e; hence, the variation of θ_e demonstrates the redistribution of atmospheric energy by organized convection. Before frontal passage, values of θ_e were large (>352 K) in the PBL. Conversely, relatively small values of θ_e were found at the 500-mb level, resulting from advection of low-θ_e air in the middle troposphere from the mainland of China. This θ_e dis-

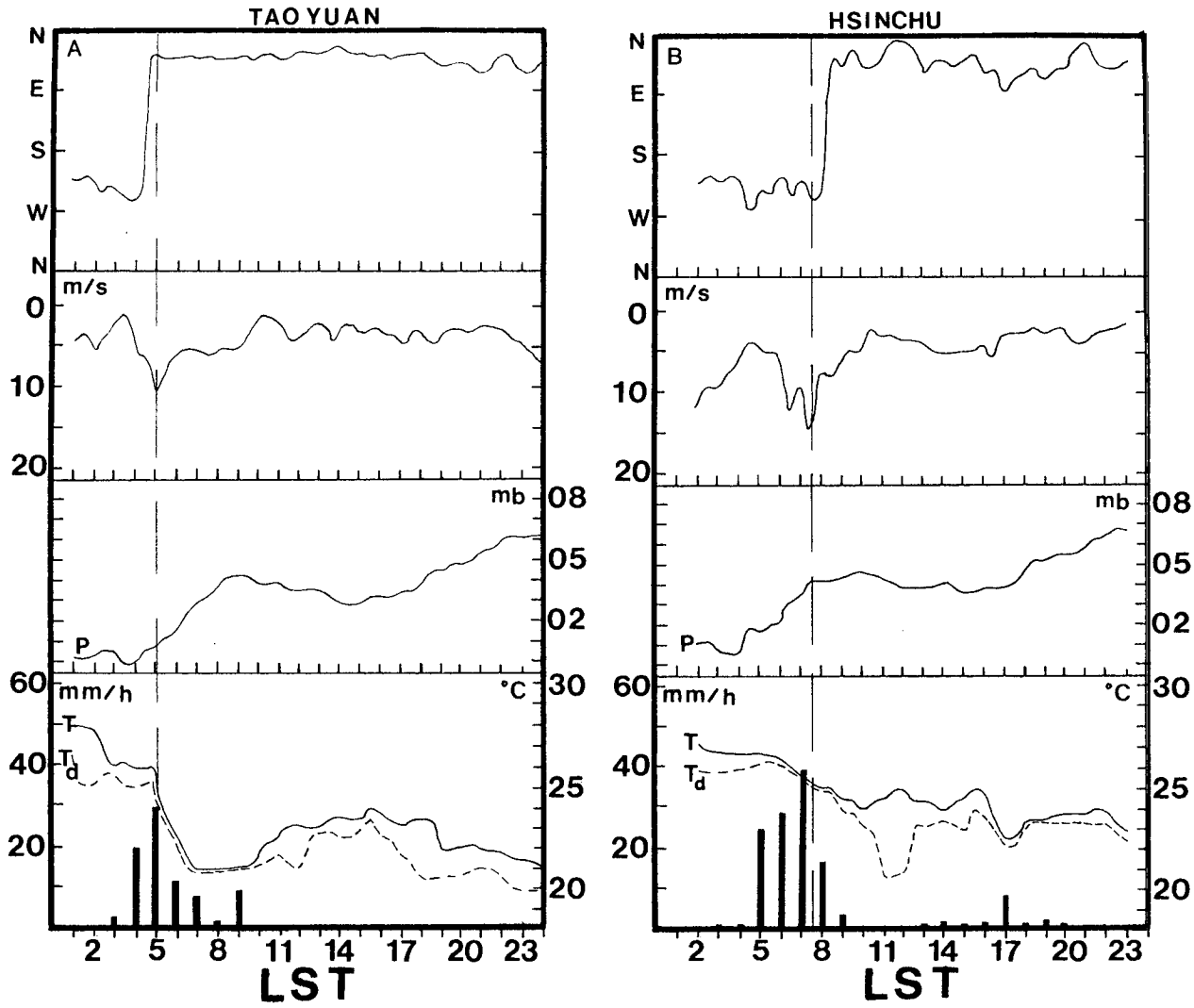

FIG. 7. Surface observations taken at (a) Taoyuan and (b) Hsinchu on 25 June, showing the wind direction, speed, pressure, temperature (solid), dewpoint (dashed), and rainfall rate. The vertical dashed line indicates the time of frontal passage.

tribution is quite common during the Mei-Yu season with abundant moisture in the lower troposphere, associated with the southwest monsoon and cooler, drier air in the mid- and upper troposphere. By contrast, values of θ_e decreased drastically from 358 to 334 K by 1400 LST 25 June during the postfrontal period. A strong θ_e gradient formed in the PBL due to the arrival of cooler and drier air from northern China. The depth of this cold air in conjunction with the Mei-Yu front was quite shallow (1–2 km). This is characteristic of a Mei-Yu front (e.g., Chen et al. 1989; Trier et al. 1989).

b. Prefrontal and postfrontal conditions

As noted earlier in section 2, the cold front passed through Panchiao at 1500 UTC 24 June. Accordingly, the Panchiao soundings released at 1200 and 1800 UTC 24 June can be used to describe the state of prefrontal and postfrontal environmental conditions, respectively. The prefrontal environment (Fig. 12a) was characterized by veering of the winds with height throughout the whole troposphere, showing large-scale warm advection in the warm sector. Moisture was available in the lower troposphere with relatively dry air in the midtroposphere. The sounding exhibited conditional instability with the freezing level near 5.5 km. A moist adiabat (dotted line) denotes the ascent of an undiluted parcel from the cloud base. In the absence of mixing with the environment, this parcel (after about 100 mb of lifting) would ascend freely above 200 mb. After frontal passage (Fig. 12b), the environmental conditions changed significantly, becoming more stable than before. The environmental wind at 900 mb reduced in speed considerably to 4–5 m s^{-1}

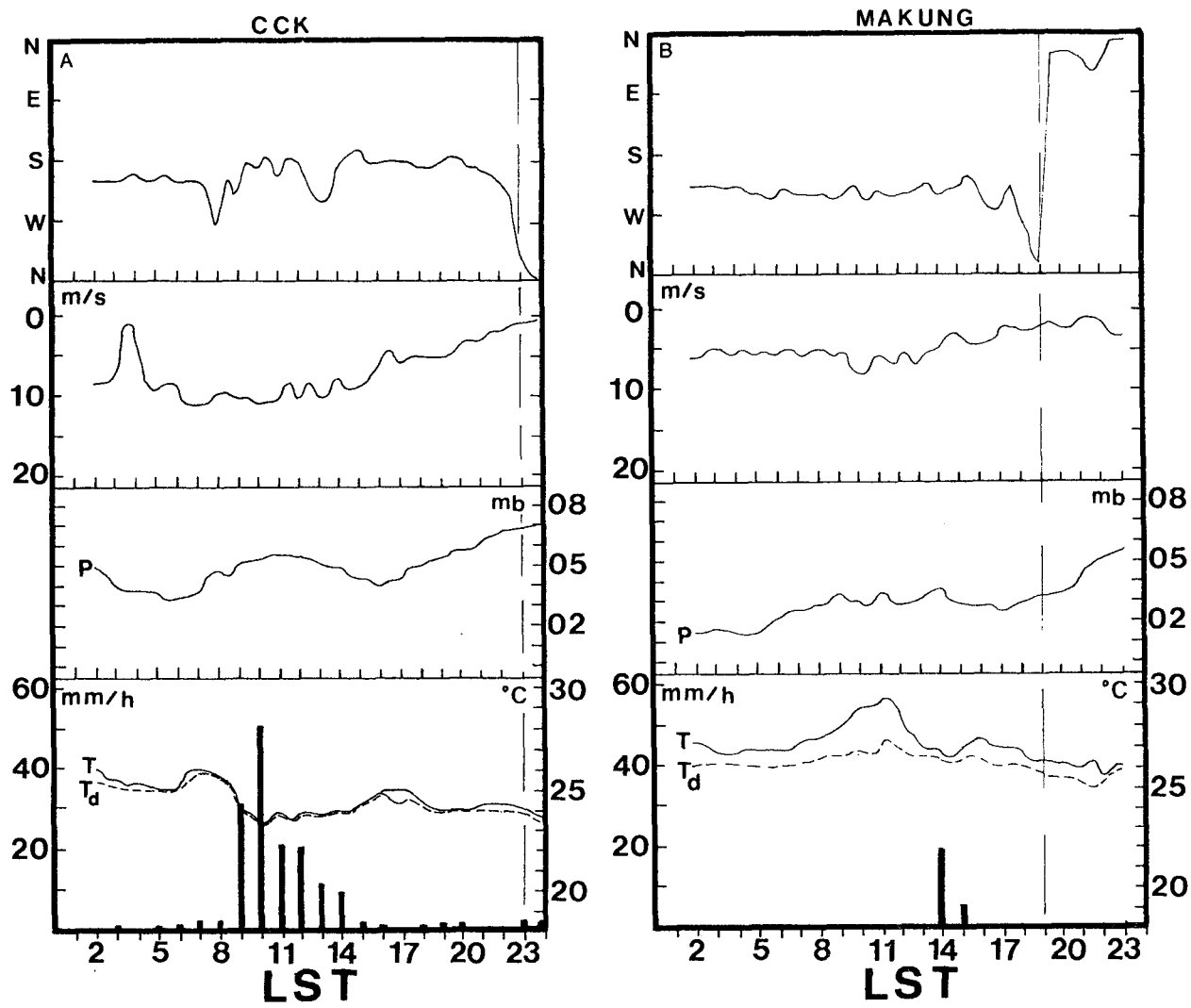

FIG. 8. As in Fig. 7 except for (a) CCK (Ching-Chung-Kang) and (b) Makung.

and was from the northwest. In the mid- and upper troposphere the winds were from the northwest and north, carrying much drier and cooler air from the mainland of China to northern Taiwan and its vicinity.

The mean environmental winds at Makung, averaged over the period from 1800 UTC 24 June to 0000 UTC 25 June, are shown in Fig. 13. Line motion during the times of dual-Doppler analysis was from 330° at 2.5 m s^{-1} (see the arrow in Fig. 13). This system speed was much slower than that of a subtropical squall line (16.5 m s^{-1}) studied by Lin et al. (1990) and Wang et al. (1990) during TAMEX IOP 2. We believe that the rapid decrease in mean wind to 5 m s^{-1} at 900 mb after frontal passage (see Figs. 10b and 12b) is the main reason for slow line motion. It will be shown later that cell motion is different from line motion. Most cells propagate at speeds faster than the line motion of 2.5 m s^{-1}. Note that the LLJ with maximum speeds of 15 m s^{-1} prevailed in the PBL below 1 km. The orientation of the jet was almost parallel to the line of convection (see the heavy dashed line in Fig. 13). The intersection angle between the line and the LLJ axis was about 8°–10°. Veering occurred at most levels, showing the large-scale warm advection throughout the whole troposphere favorable for MCS development (e.g., Maddox 1980).

With the aid of Fig. 13, profiles of the system-relative mean wind normal to the line (V_n) and parallel to the line (V_t) are presented in Fig. 14. A positive value of V_n represents flow away from the band, and a negative value of V_n represents inflow to the band. Positive values of V_n in the middle and upper layers were associated with the northwesterly and northerly winds blowing from northern China, while negative values of V_n in the lower layer corresponded to the southwest monsoon flow with the LLJ at 0.7 km. Notice that a negative V_n

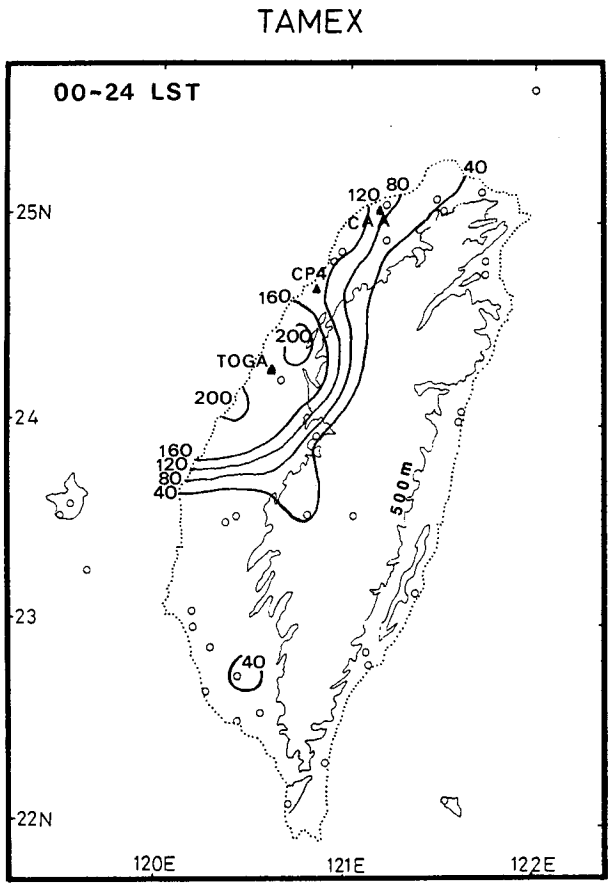

FIG. 9. The accumulated amount of rainfall in 24 h on 25 June over the island. Contour interval is 40 mm per 24 h. The locations of three 5-cm Doppler radars are indicated. The 500-m contour for the CMR is superimposed.

value of 4–5 m s^{-1} in the PBL indicates the cross-frontal inflow from the warm side of the front. This inflow causes the low-level convergence at the wind-shift line resulting in large-scale upward motion (Jou and Deng 1990). Vertical shear of V_n was moderate and positive from the surface to 6 km and remained small higher up. This pattern is quite different from that reported in the study by Wang et al. (1990) for TAMEX IOP 2 (see their Fig. 10 for comparison). For example, the profile for V_n during IOP 2 shows negative values (front-to-rear flow) at most levels in contrast to that shown in Fig. 14 (rear-to-front flow) for IOP 13, except in the lower layer.

The V_t component had positive values below 8 km and negative values above. The largest value occurred at the LLJ level near 1 km. Very large vertical shear formed in the layer below and above the LLJ. Positive values of V_t were associated with the southwesterly and westerly winds in the lower and midtroposphere, while negative values corresponded to the northwesterly and northerly winds in the upper troposphere.

4. Data analysis and computational procedures

As described in section 1, three 5-cm Doppler radars were positioned along the northwest coast of Taiwan (Fig. 1). The baseline between CP-4 and TOGA was 45 km. Specifications of the two radars can be found in Table 2 of Wang et al. (1990).

Two volume scans at 0653 and 0700 LST 25 June were obtained from the CP-4 and TOGA radars. We employed the data analysis and reduction procedures similar to that reported in studies by Lin et al. (1986) and Wang et al. (1990) to process dual-Doppler data. Only those data with high signal-to-noise ratio values were accepted in the analysis. These data were collected into 10 slabs of varying vertical depth whose mean altitudes range from 0.75 to 9.75 km. All variables within a slab were objectively interpolated onto horizontal Cartesian grids (40 × 36) using a 2.5-km scan radius. Note that there is filtering inherent in this objective analysis scheme especially for mesoscale perturbations with wavelength less than 3 km. The grid spacing was 1 km in all three directions. Vertical velocities were calculated from the anelastic continuity equation by integrating downward from the top using the horizontal winds. The derived three-dimensional winds were subjected to variational adjustment to render them internally consistent (see Lin et al. 1986 for details).

The derived wind field is subject to both random and nonrandom errors. Using the technique similar to that of Wilson et al. (1984), we found the combined errors due to statistical uncertainty in the radial velocity estimates and geometrical considerations to be 1–2 m s^{-1} for the horizontal-derived winds.

For the vertical velocity calculation, the uncertainty in the w estimate is more difficult to determine since it is closely related to errors in horizontal divergence, boundary conditions, etc. Sources of errors in the w estimate were described in the study by Wang et al. (1990). However, the variational adjustment of winds has reduced errors in the w estimates considerably (Lin et al. 1986). We estimate that the errors in accuracy of w in this study would be 10%–20% of the value in the largest updrafts at the height of their maxima.

5. Discussion of results

As noted earlier, two volumes of dual-Doppler data at 0653 and 0700 LST 25 June were considered in the present study. During the times of analysis, the system traveled from 330° at 2.5 m s^{-1}. Since the system moved so slowly, flow fields presented in the fixed frame are nearly the same as those in the line-relative or system-relative frame. In the following, all flow fields are presented in the system-relative coordinates with a constant speed of 2.5 m s^{-1} from 330°. Because the system exhibited some similarities in structure between the two analysis times, only the results at 0653 LST are presented to avoid redundancy.

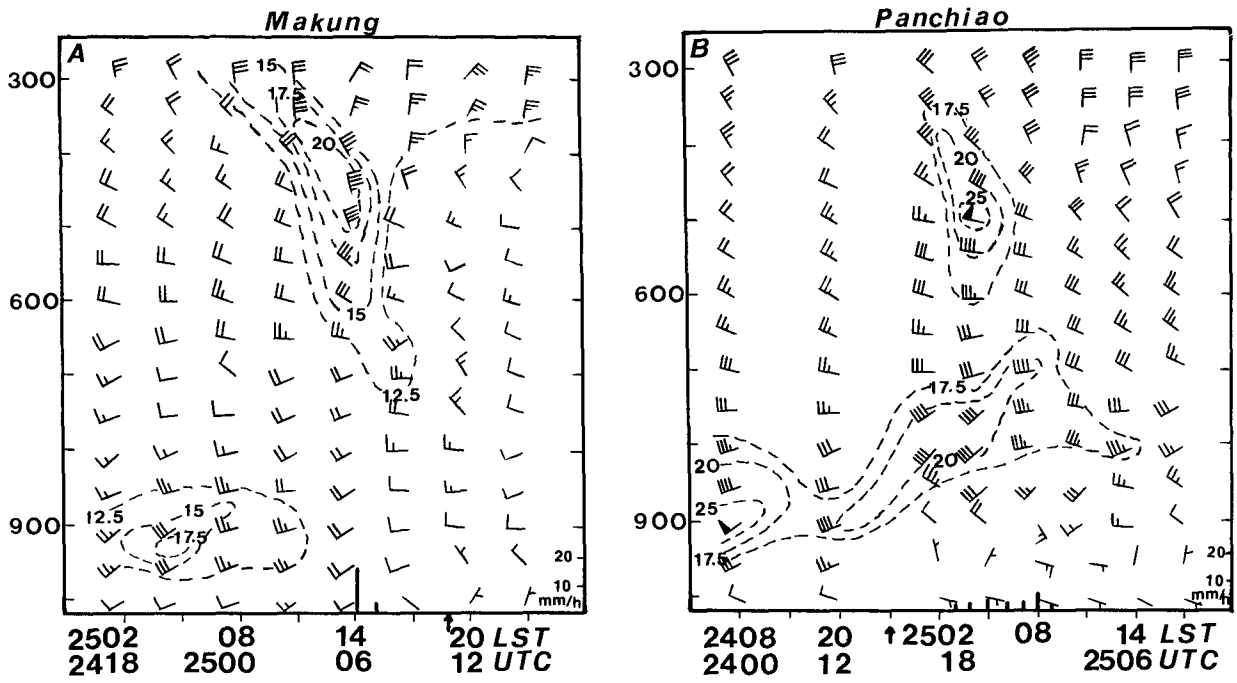

FIG. 10. Time–height variations of rawinsonde winds at (a) Makung and (b) Panchiao on 24–25 June. The dashed line represents an isotach in units of meters per second (m s^{-1}). The arrow shows the time of frontal passage. The vertical solid bar along the time axis shows the precipitation rate (mm h^{-1}).

a. Distribution of radar reflectivities in convective rainband

Figure 15 displays spatial variations of the reflectivity field Z at various analysis levels from 0.75 to 8.75 km for 0653 LST. This field is subject to the filtering inherent in the objective analysis scheme considered (see section 4). All heights in this study are AGL. For the purpose of illustration, the wind-shift line at the lowest two levels is superimposed (see the heavy dashed line in Fig. 15). This wind-shift line corresponds well to the position of the Mei-Yu front (see section 5b for details). It is seen that reflectivities are not homogeneous on the warm side of the wind-shift line. Values of Z range from 20 to 40 dBZ with the maxima located in a narrow band on the southeast side of the wind-shift line. This prefrontal convective rainband is oriented in the direction almost parallel to the wind-shift line. The height of 20-dBZ contour (see the dash–dot line in Fig. 15) reaches 9 km and higher. There are many cells embedded within the rainband (see the shaded area $Z > 30$ dBZ in Fig. 15) with relatively weak reflectivity regions in between.

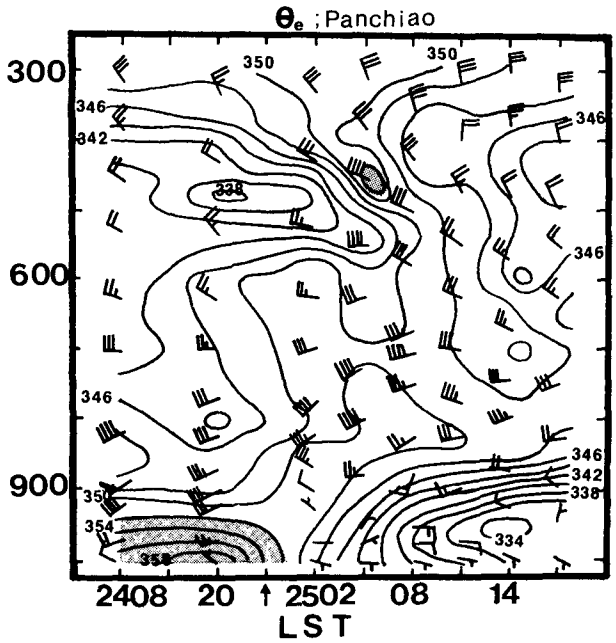

FIG. 11. Time–height variations of equivalent potential temperature θ_e at the Panchiao station near Taipei on 24–25 June. Contour interval for θ_e is 2 K. The shaded area denotes $\theta_e > 352$ K.

Examination of Fig. 15 further reveals that stronger reflectivities occur in the lower and middle layers with maxima near 3.75 km. Values of Z decrease rapidly at levels above 4.75 km. This finding is similar to that of TAMEX IOP 2 (Wang et al. 1990), TAMEX oceanic convection on the east side of Taiwan (Jorgensen and LeMone 1989), and GATE [GARP (Global Atmospheric Research Program) Atlantic Tropical Experiment] (Szoke et al. 1986), except our magnitudes are somewhat smaller with the maxima less than 40 dBZ. According to Jorgensen and LeMone (1989), the oceanic convection in GATE and TAMEX is dominated by warm-rain coalescence process below the

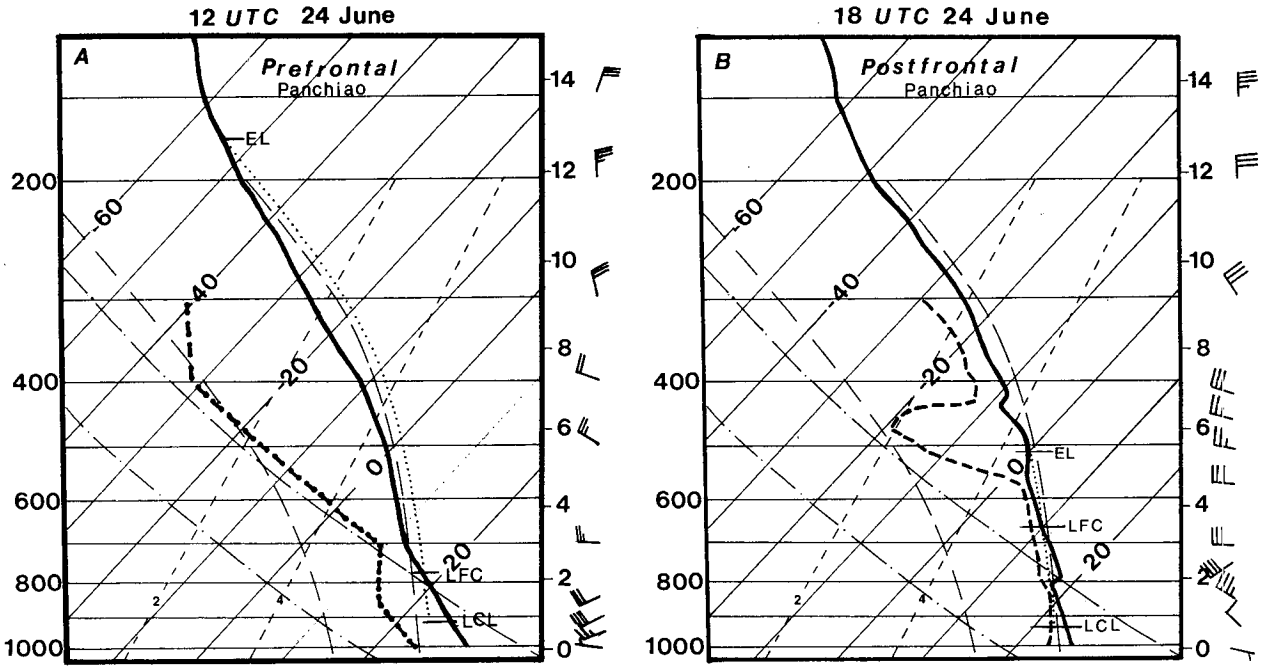

FIG. 12. The environmental sounding at (a) 1200 UTC 24 June for the prefrontal atmosphere and (b) 1800 UTC 24 June for the postfrontal atmosphere at Panchiao near the city of Taipei over northern Taiwan. The lifting condensation level (LCL), the level of free convection (LFC), and the equilibrium level (EL) are also indicated.

freezing level (~4–5 km). It will be shown later that the warm-rain process in IOP 13 appears to produce relatively weak convective downdrafts in the high-reflectivity regions ahead of the wind-shift line rather than behind it. This is quite different from the squall-line case in TAMEX IOP 2 (Wang et al. 1990). Because

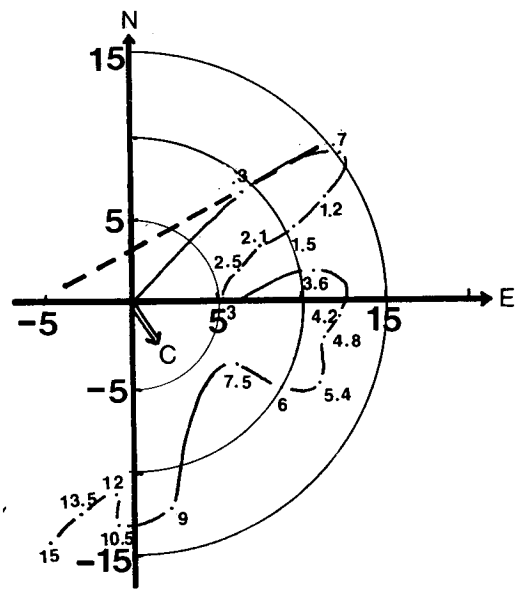

FIG. 13. The environmental mean winds at various heights in kilometers in the prefrontal environment. The mean wind is the average of three Makung soundings at 1800 and 2100 UTC 24 June and 0000 UTC 25 June. The heavy dashed line shows the orientation of a convective line. The system was moving at 2.5 m s^{-1} from 330° (see the arrow).

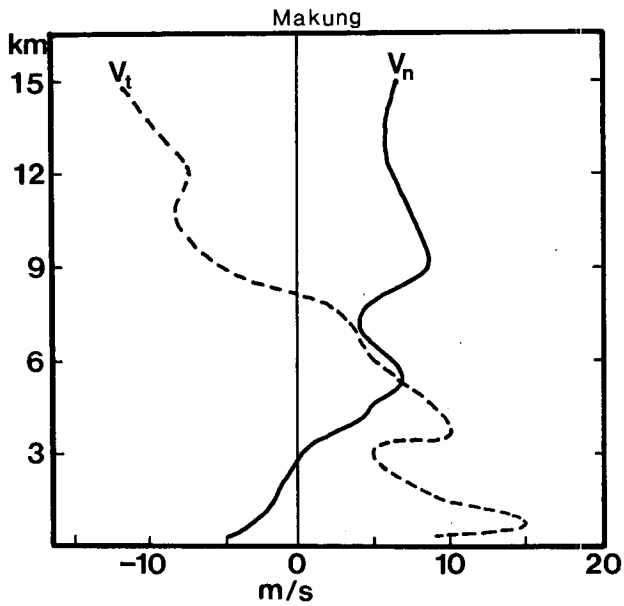

FIG. 14. Profiles of the system-relative mean wind normal to (V_n) and parallel to (V_t) the convective rainband in the prefrontal environment. These components are extracted from Fig. 13. A positive value of V_n is toward the south-southeast (150°) in the direction of system movement (C), while V_t is positive toward the east-northeast (60°).

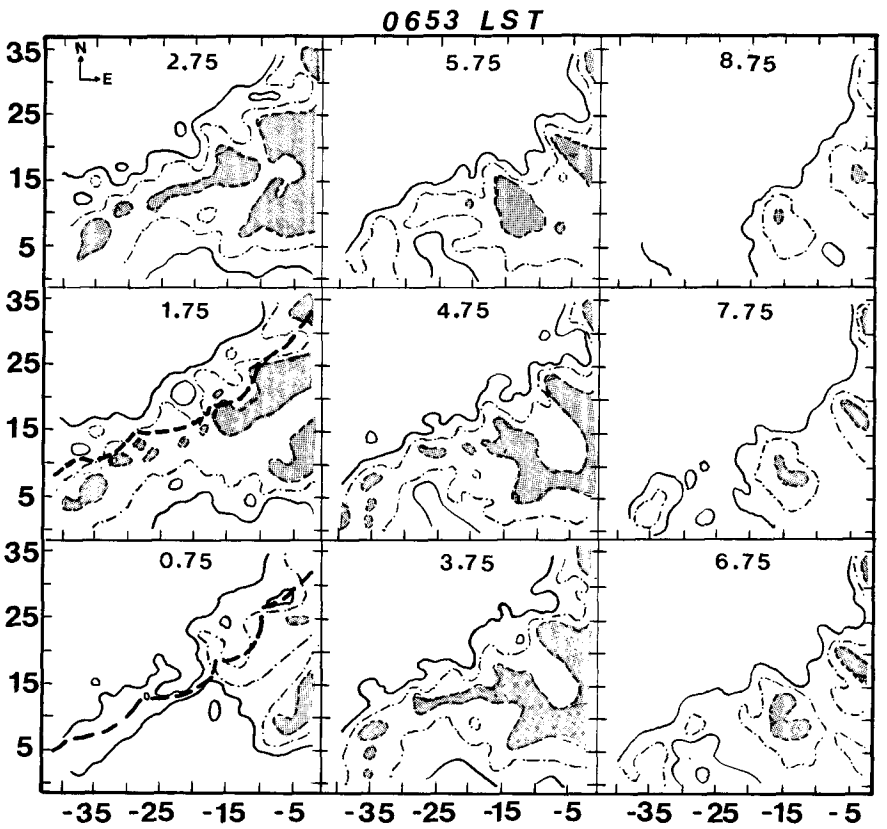

FIG. 15. Horizontal variations of reflectivity Z at various heights for 0653 LST 25 June as determined from dual-Doppler analyses. The heavy dashed line indicates the approximate location of the cold front. Contour interval is 10 dBZ starting from 10 dBZ. The shaded area shows $Z > 30$ dBZ. Distances are in kilometers from the TOGA radar.

of the prevailing westerly and northwesterly flow in the middle and upper troposphere, the reflectivity cores are elongated southeastward with the shear vector. The convective downdraft, developed in the elongated high core region on the southeast side of the front, produces the low-level outflow to form a gust front ahead of the convective rainband. This gust front in turn initiates new convection ahead of the old convection, thereby prolonging the life span of the rainband. The rainband, located approximately 12–15 km southeast of the wind-shift line as seen at 1.75 km (Fig. 15), is attributed to the new convection previously mentioned. Its orientation is almost parallel to the primary rainband ahead of the wind-shift line.

b. Horizontal view at 0653 LST

Figure 16 shows fields of the horizontal (system-relative) wind with reflectivity contours superimposed at 0.75 and 1.75 km. Distances are in kilometers from the TOGA radar (T). At 0.75 km (Fig. 16a), a distinct line of wind shift (heavy dashed line) is seen. This line matches well with the position of the Mei-Yu front and exhibits a wavy pattern. The wavelength of these mesoscale disturbances is of the order of 11 km. According to Carbone (1982, 1983), strong low-level horizontal shear of the horizontal winds across the cold front resulted in small-scale vortices at about 13-km intervals along the gust front. A wavy pattern on the mesoscale cold front was also found in the study by Hobbs and Persson (1982) for a midlatitude cold-frontal rainband. In Part II of this study, we will discuss the mesoscale structural features of the wind-shift line and Mei-Yu front in details using the derived three-dimensional Doppler winds and retrieved pressure and temperature perturbations.

On the south side of the front, a secondary wind-shift line (thin dashed line) was also evident ($-40 < x < -18$ km). It will be shown later that this secondary wind-shift line is associated with the gust front that resulted from the convective downdraft in the high-reflectivity region ahead of the leading edge of the front. To the southeast of the gust front, new cells develop similar to those observed in IOP 2 (Wang et al. 1990).

Inspection of Fig. 16 further reveals that the winds are predominantly from the southwest in the areas southeast of the line, representative of the southwest monsoon flow. Behind the front the winds become

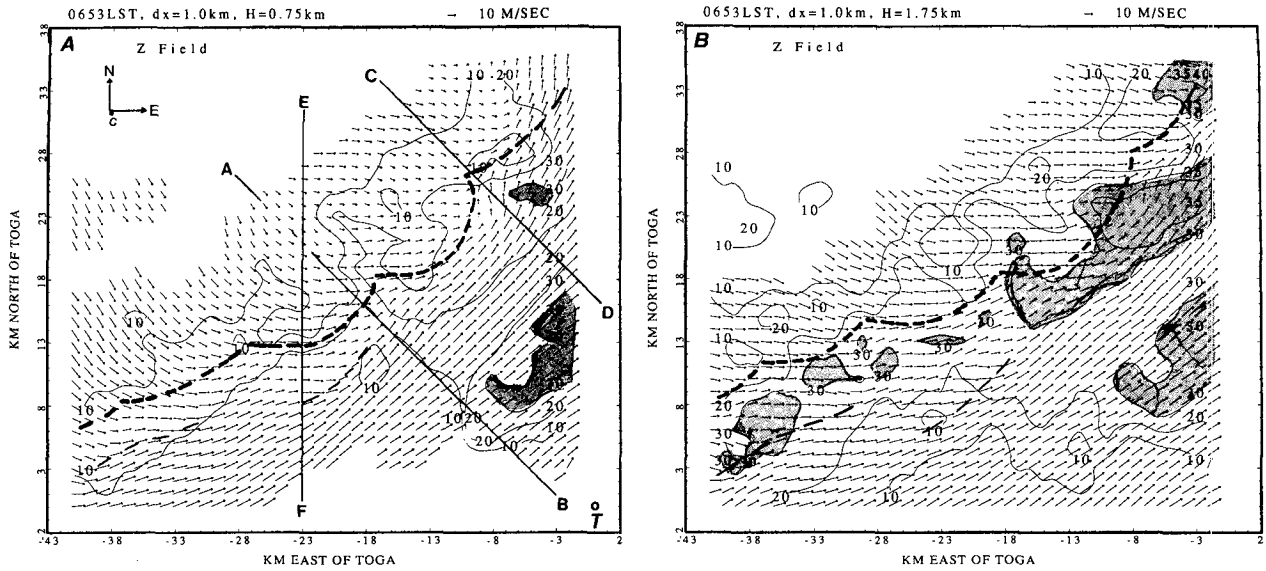

FIG. 16. Fields of the horizontal system-relative wind with reflectivity contour superimposed for (a) 0.75 and (b) 1.75 km at 0653 LST 25 June. Reflectivities greater than 30 dBZ are shaded. The heavy dashed line shows the wind-shift line, corresponding to the position of the Mei-Yu front, while the thin dashed line denotes the gust front (GF). North (N), east (E), system motion (C), and TOGA (T) are indicated. Lines *AB*, *CD*, and *EF* in Fig. 16a signify the vertical cross sections normal to the front to be presented in Figs. 21–23.

northwesterly, carrying much cooler air from northern China. The low-level convergence occurs along the wind-shift line (Fig. 17a). The magnitude of horizontal convergence/divergence is of the order of 5×10^{-3} which is smaller than that of Carbone (1982). A secondary wind-shift line (thin dashed line) is also accompanied by the strong horizontal convergence. As a result of the horizontal convergence along the wind-shift line, organized convection develops on the warm side of the Mei-Yu front. A narrow band of high reflectivities, located in a broad area ahead of the front, is evident at 1.75 km (Fig. 16b). This convective rainband consists of many cells and is oriented in an east-northeast–west-southwest direction parallel to the front. Reflectivities within the rainband are not homogeneous with values varying from 20 to 38 dBZ. The maximum reflectivity at this level is about 38 dBZ, which is smaller than that observed in a subtropical squall line

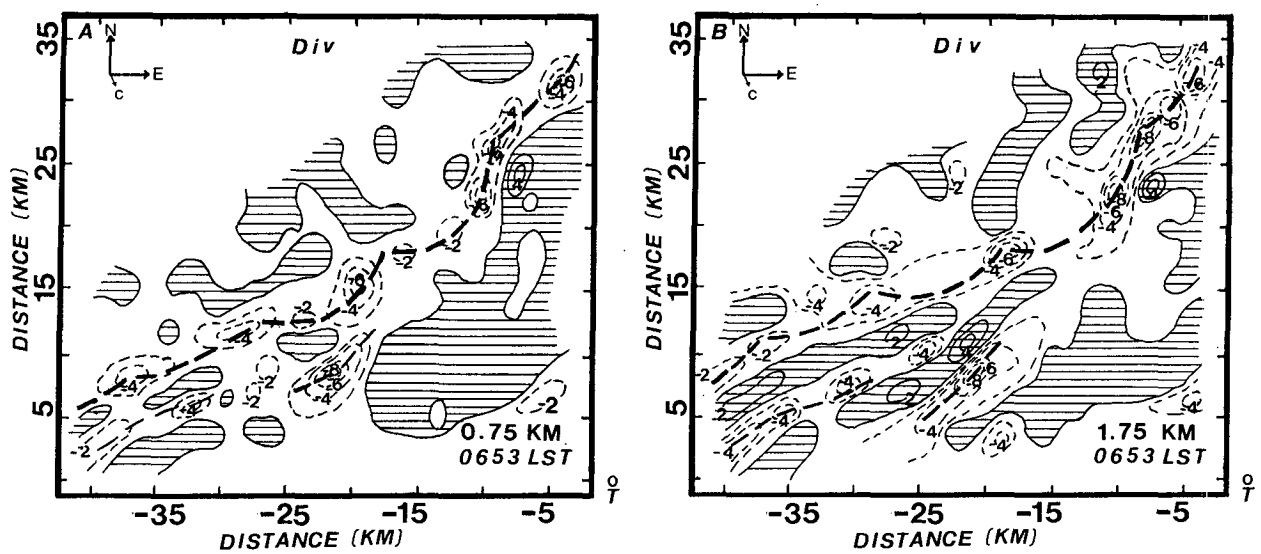

FIG. 17. As in Fig. 16 except for horizontal convergence/divergence. Contour interval is 2×10^{-3} s^{-1} with positive values (divergences) hatched.

during TAMEX IOP 2 (e.g., Lin et al. 1990; Wang et al. 1990). By contrast, reflectivity decreases rapidly behind the wind-shift line. The 10-dBZ reflectivity contour is nearly parallel to the front. The horizontal convergence along the wind-shift line is still strong at this level (Fig. 17b). Similarly, the gust front (thin dashed line) is located in the zones of strong convergence. On the other hand, the horizontal divergence dominates in the areas outside of the wind-shift lines. The magnitude is much weaker than that of the horizontal convergence. Note that the horizontal divergences (hatched) in the narrow areas between the cold front and the gust fronts are associated with the convective downdrafts due to rain loading.

Our findings as a whole are in good agreement with those reported in the study by Trier et al. (1989). Using the TAMEX single-Doppler data gathered on 8 June, they found that the enhanced rainband, coincident with the wind shift, was caused by frontal lifting. Widespread but less intensive precipitation was present ahead of the wind-shift line. The main difference between the two studies, however, is due to the position of the convective rainband. Ours was located on the warm side of the Mei-Yu front with more stratiform rain toward the cold side. Conversely, their convective rainband was located on the cold side of the surface frontal position. We believe that the environmental winds may have played the role in affecting the position of the rainband as explained before.

The horizontal (system-relative) wind fields at 4.75 and 7.75 km are presented in Fig. 18. Note that the wind-shift line is no longer apparent at these two levels and levels in between (not shown). However, the convective rainband is still evident. There are many cells embedded within the rainband with maximum reflectivities reaching 30 dBZ at 7.75 km (Fig. 18b). The reflectivity cores of this rainband appear to be elongated toward the southeast with the vertical shear of the horizontal environmental winds as depicted in Fig. 13. A somewhat similar pattern was reported in the study by Lemaitre et al. (1989) over southwestern France based on dual-Doppler data. They found that a rainband was oriented along the surface front and was nearly normal to the vertical shear of the environmental wind with high-reflectivity cores elongated in the direction of the environmental shear vector.

Horizontal distributions of vertical velocity at 0.75 and 1.75 km are shown in Fig. 19. In the PBL, all first derivatives in radial velocity including divergence, vorticity, and deformation are of the order of 5×10^{-3} s^{-1} with extreme values of $\pm 10^{-2}$ s^{-1} along the wind-shift line. These magnitudes are smaller than those reported in the study by Carbone (1982). Note that upward motion dominates in the zones along the wind-shift line. The maximum updraft speed is about 4 m s^{-1} at this level. It increases considerably at 1.75 km (Fig. 19b). On the other hand, upward motion in the area behind the front is relatively weak with a maximum of less than 4 m s^{-1}. Examination of Figs. 16 and 19 reveals that many convective downdrafts occur in the high-reflectivity regions. This finding suggests that rain loading may have played an important role in initiating and maintaining the downdrafts. Similar findings were reported in other TAMEX studies by Jorgensen and LeMone (1989) and Lin et al. (1990).

Figure 20 displays fields of vertical velocity at 4.75 and 7.75 km. Upward motion dominates in the convective rainband with maximum values in excess of 8

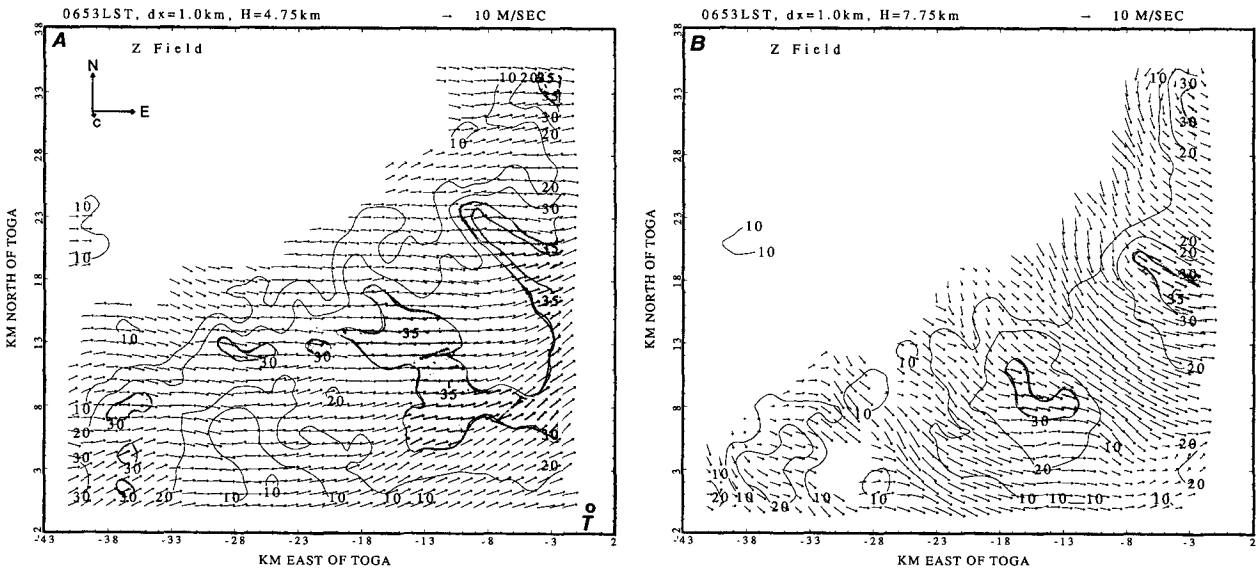

FIG. 18. As in Fig. 16 except for (a) 4.75 and (b) 7.75 km.

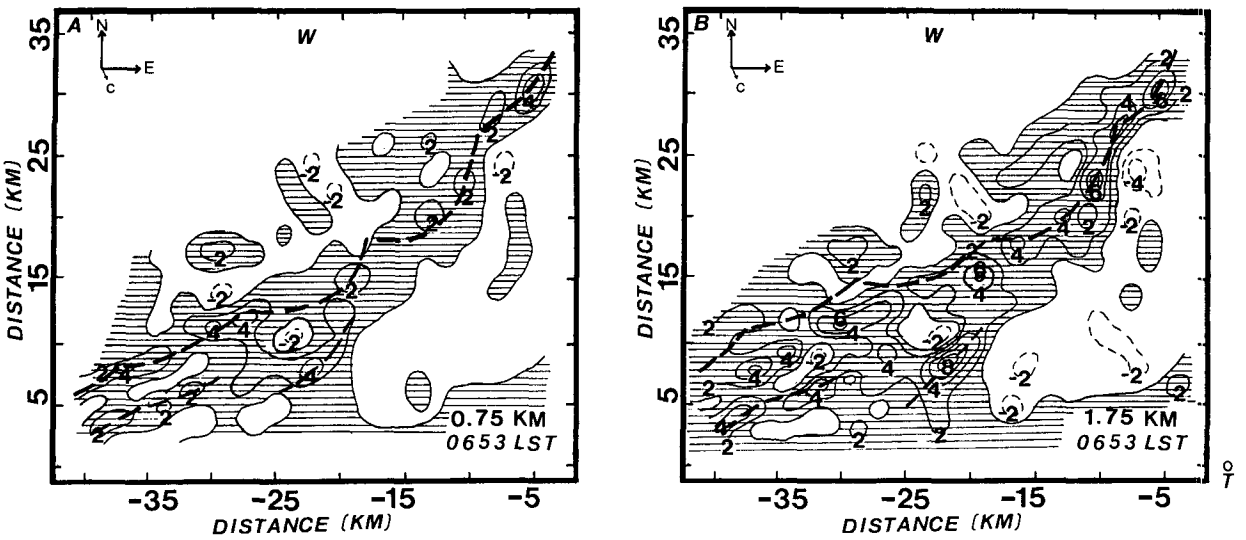

FIG. 19. Fields of vertical velocity for (a) 0.75 and (b) 1.75 km at 0653 LST 25 June. The heavy dashed line shows the wind-shift line. Contour interval is 2 m s^{-1} with positive values hatched.

m s^{-1} (Fig. 20a). At 7.75 km (Fig. 20b), upward motion is much weaker. However, several individual cells with maximum reflectivities of 30 dBZ or greater (Fig. 18b) are visible. Like the reflectivity fields in Fig. 18, both convective updrafts and downdrafts are also elongated toward the southeast in the direction nearly perpendicular to the rainband. The prevailing flow at the 7.75-km level is from the northwest at stronger speeds, resulting in an elongation of reflectivity cores toward the downwind (southeast) direction. This result is quite different from that of the subtropical squall line reported in studies by Wang et al. (1990) and Lin et al. (1990).

c. *Vertical cross section*

The flow field and vertical velocities along line AB in Fig. 16a are depicted in Fig. 21. Reflectivity contours in intervals of 10 dBZ are superimposed. The heavy dashed line shows the approximate location of the frontal boundary. The leading edge of the front is located at $x = -18$ km and $y = 16$ km. To the southeast

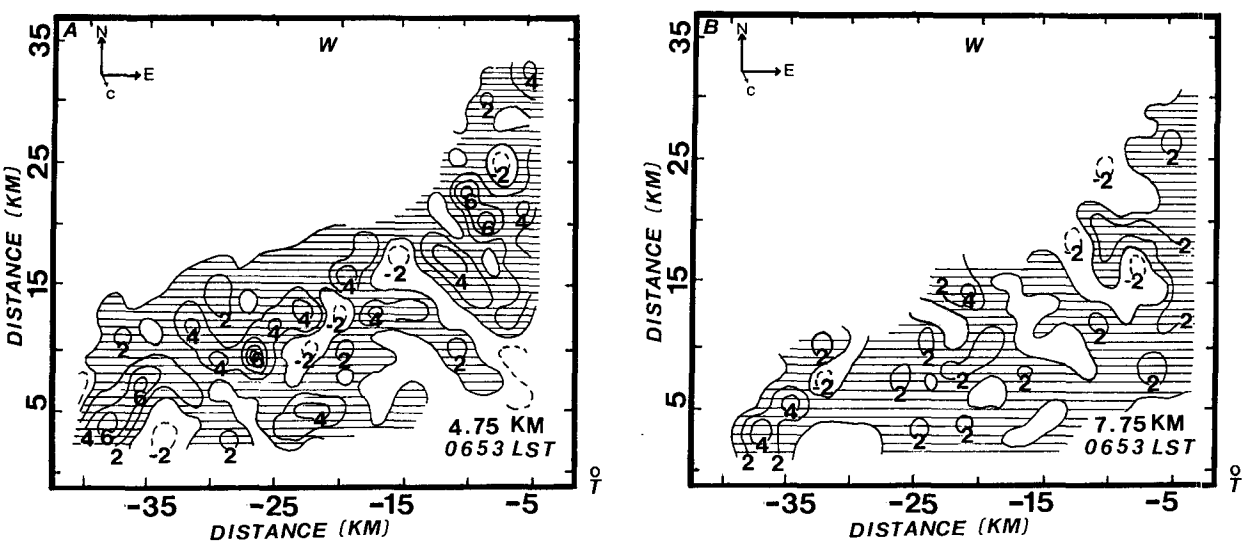

FIG. 20. As in Fig. 19 except for (a) 4.75 and (b) 7.75 km.

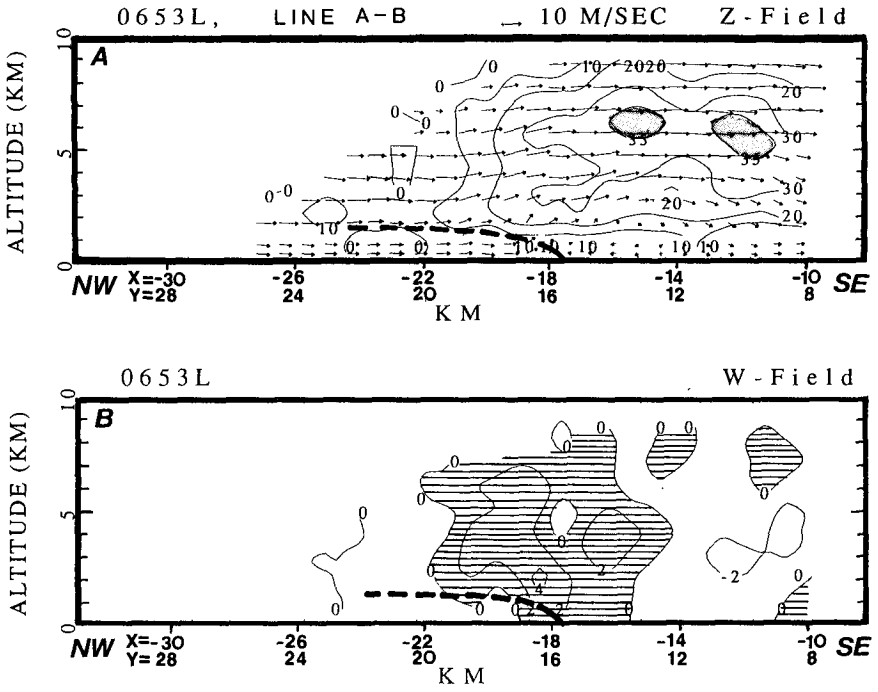

FIG. 21. The vertical cross section along line *AB* in Fig. 16a, showing (a) the system-relative winds with reflectivity contours superimposed and (b) vertical velocity (w) at 0653 LST 25 June. The frontal boundary is signified by the heavy dashed line. Contour interval for w is 2 m s^{-1} with positive values hatched. Reflectivities greater than 35 dBZ are shaded.

of the front (right side of the figure), the winds are from the southwest and west in the lower and middle troposphere and become northwesterly in the upper troposphere. The southwesterly flow at low levels transports high-θ_e environmental air toward the wind-shift line. The updraft is weak ($W_{max} < 5$ m s^{-1}) and tilted slightly toward the northwest (left side of the figure) along the frontal boundary (heavy dashed line). The convective downdraft is relatively weak in a broad area ahead of the front. It occurs in the areas of high reflectivity within the rainband.

The precipitation is deep but not intense in the regions ahead of the front. The reflectivity maxima (shaded) are aligned perpendicular to the front and along the environmental shear vector. The elongated reflectivity core is responsible for initiating the convective downdraft near $x = -12$ km and $y = 10$ km (Fig. 21b). The maximum reflectivity within the convective rainband is less than 40 dBZ. The 10-dBZ contour reaches the height of 10 km and higher. By contrast, the precipitation behind the leading edge of the front is rather shallow, having the height of the 10-dBZ contour in the 2–3-km layer (Fig. 21a). These results show two types of precipitation in the regions separated by the front, that is, the convective type in front and stratiform type behind.

Figure 22 shows the flow and vertical velocity fields along line *CD* in Fig. 16a. This cross section and the one discussed before are both oriented in the direction nearly perpendicular to the front. The convective updraft forms at the leading edge of the front (heavy dashed line) with a maximum speed of 6 m s^{-1}. In the high-reflectivity regions on the warm side of the front (right side of the figure), convective downdrafts prevail. The convective downdraft at $x = -2$ km and $y = 19$ km results in a low-level diverging flow. Part of this diverging flow moves toward the southeast and meets with the advancing moisture-rich air from the warm side of the front at $x = -1$ km and $y = 18$ km, producing a secondary updraft ahead of the gust front (see the arrow in Fig. 22). This secondary updraft eventually becomes a new cell ahead of the old (main) cell. This point will be further illustrated later. In the middle and upper layers, the northwesterly flow dominates, shifting the reflectivity cores toward the southeast. These elongated reflectivity cores are responsible for initiating the convective downdrafts in a broad area 3 km southeast of the surface front. The downdraft located at $x = -6$ km and $y = 23$ km coincides with one of the high-reflectivity cores (see the shaded area in Fig. 22). Recall that the prevailing environmental flow on the warm side of the front is from the southwest (Fig. 16). This monsoon flow will continue to carry moisture-rich air from the South China Sea toward the wind-shift line as mentioned before. As a result, the convection at the leading edge of the front continues. Further, new con-

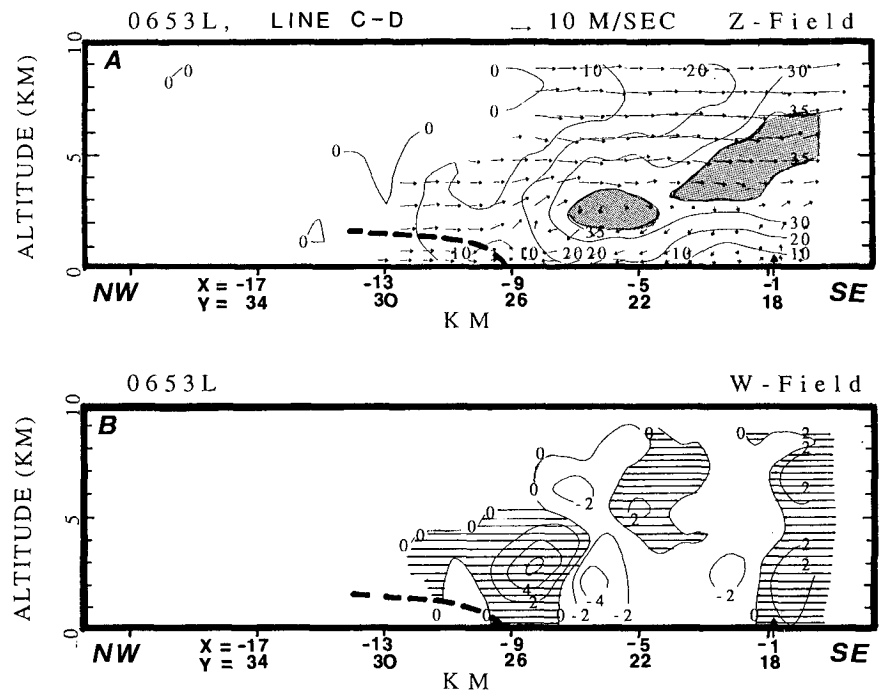

FIG. 22. As in Fig. 21 except for the cross section along line *CD* in Fig. 16a. The arrow indicates the gust front (GF).

vection develops on the southeast side of the front ahead of the precipitation-induced convective downdraft. This mechanism appears to be largely responsible for maintaining the life cycle of the rainband.

The north–south cross section along line *EF* in Fig. 16a in the direction nearly normal to the front is displayed in Fig. 23. On the warm side of the front (right side of the figure), the southerly wind associated with the southwest monsoon prevails from the surface to 5 km. In the PBL, this inflow transports high-θ_e air from the southwest toward the wind-shift line. Behind the front, the northerly wind associated with the northwesterly flow dominates, carrying much cooler low-θ_e air from northern China. It collides with the high-θ_e air at y = 13 km, resulting in upward motion at the leading edge of the front (see the heavy shaded area, $w > 4$ m s^{-1}, in Fig. 23). Part of the inflow continues to travel toward the north above the frontal boundary (heavy dashed line). The vertically transported air within the updraft column merges with the northwesterly flow in the upper layer ($z > 5$ km), forming an elongated reflectivity core toward the southeast as noted earlier. The convective downdraft (D) with a maximum speed of -4 m s^{-1} develops in the high-reflectivity region near y = 10 km. As the descending air of this downdraft reaches the ground, it spreads out horizontally. The northward part of the outflow enhances the convergence at the leading edge of the front (y = 13 km). The southward part, on the other hand, meets with the incoming high-θ_e air at y = 9 km, resulting in upward motion in the area south of the gust front (GF) at y = 9 km. This new cell is located about 5–8 km south of the leading edge. It is not in the area of high reflectivity. At the time of analysis, this new cell had just formed and did not produce precipitation yet. It is of interest to see the evolution of this new cell using single-Doppler data obtained from TOGA. We plan to present our findings in a future report.

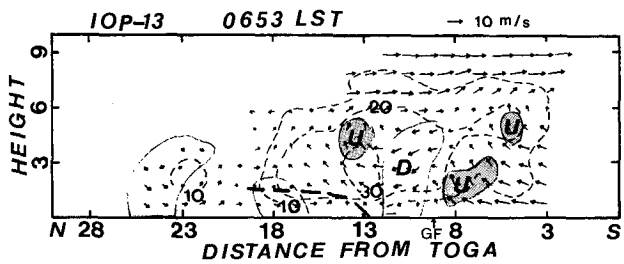

FIG. 23. The north–south cross section along line *EF* in Fig. 16a showing the system-relative winds with reflectivity contours superimposed at 0653 LST 25 June. The area with downward motion is lightly shaded. The heavy shaded area signifies the convective updraft with $w > 4$ m s^{-1}. The cores of convective updraft and downdraft are labeled U and D, respectively.

Inspection of Fig. 23 further reveals that the northerly wind is confined to the layer below 2 km. It shows that the depth of the cold air associated with the Mei-

Yu front being investigated is shallow. This finding is consistent with that reported in other TAMEX case studies. For example, Chen et al. (1989) showed a decrease in the depth of the cold air, associated with the front, as it moved off the coast of China. The front had a depth of 1 km in the vicinity of Taiwan. Using the velocity–azimuth display (VAD)–derived winds, Trier et al. (1990) found that the depth of the cold air associated with a Mei-Yu front in TAMEX IOP 8 is about 2 km. However, the absence of the rearward acceleration of the southwesterly flow over the cold air in the 2–6 layer as seen in Figs. 21–23 is different from that reported in a subtropical cold front (Trier et al. 1989) and a midlatitude cold front (Carbone 1982).

d. Comparison with other TAMEX studies

The kinematic properties of a convective rainband presented in this study are quite different from those for a subtropical squall line during TAMEX IOP 2, presented in the study by Wang et al. (1990). The squall line propagated at a rapid speed (16.5 m s^{-1}) from the southwest. The strong southwesterly environmental winds with magnitudes varying from 10 to 20 m s^{-1} prevailed in the lower and midtroposphere. The leading edge of the squall line was oriented nearly in a north–south direction. An LLJ was located in the 3–4-km layer and provided the necessary strong vertical shear at lower levels. As depicted in Fig. 24, front-to-rear environmental flow dominated at all levels on the front side of the squall line and was accompanied by shallow rear-to-front flow (1–3 km) on the back of the line. In the lower troposphere, the front-to-rear environmental high-θ_e air was lifted at the convergence zone, feeding the convective updrafts at the leading edge (heavy dashed line). The main updraft, with a maximum speed of 12 m s^{-1} ($x = -16$ km), was tilted toward the west in the lower layer and became almost erect higher up. The updraft tilt kept water loading and evaporative cooling in the updraft to a minimum from the falling rain. As the rain fell out of the updraft, it increased the density of the downdraft air below the tilted updraft. The convective downdraft on the rear of the main updraft was essential to transport cooler midtropospheric air into the lower layer. Part of the negatively buoyant air from the rear continued to move forward, colliding with the advancing high-θ_e air in the PBL. As a result, new convective cells formed ahead of the old cells, thereby prolonging the lifetime of the squall line. In the convective region, the low-level front-to-rear inflow was lifted at the leading edge to form the main updraft. The lifted air continued to flow west in the mid- and upper levels heading toward the trailing stratiform region, which is quite different from that shown in Figs. 21–23. The interaction between the convective updraft and downdraft played the role of maintaining the three-dimensional circulation within the squall line.

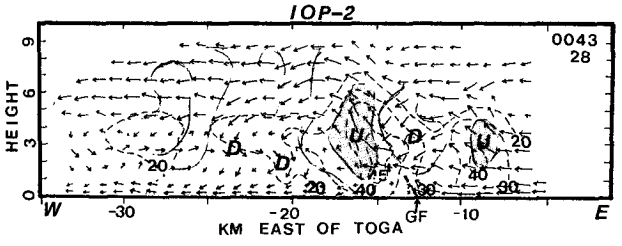

FIG. 24. The east–west cross section 28 km north of TOGA at 0043 LST 17 May during TAMEX IOP 2, showing the system-relative winds with reflectivity contours superimposed (after Wang et al. 1990). Areas with downward motion are lightly shaded. Convective updrafts with $w > 4$ m s^{-1} are shaded. Letters U and D signify the cores of convective updraft and downdraft, respectively.

The structural features of a cold front during TAMEX IOP 8 on June 1987 were reported in the study by Trier et al. (1989) using single-Doppler radar data and upper-air and surface observations. Results showed that the structure and propagation properties of a frontal system resemble those for a squall-line gust front in conjunction with the gravity–density current mechanism. The system was characterized by the moderate to high baroclinicity and abrupt wind shift associated with the front. Unlike squall-line gust fronts, this system originated in a synoptic-scale deformation zone at midlatitudes and then propagated toward the southeast at a moderate speed (~8–9 m s^{-1}). Even though the amount of convective available potential energy (CAPE) was comparably small, strong frontal lifting was adequate to sustain a quasi-steady convective system at the leading edge of the front. This feature, together with the shallow nature of the cold pool (1–2 km) and abrupt wind shift, the strong temperature and moisture gradients, and the extended rearward acceleration over the cold air, is similar to those observed in midlatitude fronts, such as the one studied by Carbone (1982) and Parsons et al. (1987).

Our findings presented in Part I of this study, to some extent, are similar to those of Trier et al. (1989) during TAMEX IOP 8, except the system we studied traveled at much slower speed (2.5 m s^{-1}) and lasted longer. The northwestly flow prevailed in the layers above 5 km resulting in an elongated precipitation core with the environmental shear vector toward the southeast. It produced very heavy precipitation (more than 200 mm in 24 h) over the west coast of central Taiwan.

In regard to the movement of a system, the influence of topography plays an important role in affecting the frontal structure and propagation speed over Taiwan and its vicinity (see section 2 for details). As explained earlier, the presence of the CMR often divides a Mei-Yu front into two parts. The eastern part over the Pacific Ocean continues to travel at a (normal) rapid speed toward the southeast, while the western part (west

and southwest of Taiwan) remains quasi-stationary, especially in the area close to the west coast of Taiwan. In this case the western portion of the front traveled at only 2.5 m s^{-1}, 3–4 times slower than the front on the east side of the CMR (Fig. 4).

A calculation of the gravity–density propagation speed similar to that of a gravity-current–driven squall-line gust front (Charba 1974) was reported in studies by Carbone (1982), Hobbs and Persson (1982), Lemaitre et al. (1989), Trier et al. (1989), etc. Our result shows that the propagation speed of 2.5 m s^{-1} is much slower than that predicted by the von Kármán (1940) speed formula. This speed is much slower than that for a subtropical squall line in TAMEX IOP 2 mentioned previously.

e. A conceptual model

Unlike the squall line in IOP 2, the prefrontal convective rainband in IOP 13 developed on the warm side of the front over northwestern Taiwan as the Mei-Yu front was approaching the northwest coast. The front retained its baroclinic character before reaching the central and southern portions of Taiwan (Trier et al. 1989). It provided lifting to initiate the convection along the cold front (see the convective updraft CU in Fig. 25). The wind-shift line was a result of the warm, moist southwest flow from the South China Sea in collision with the cool, dry northwest flow from northern China. The southwesterly flow was accompanied by a LLJ in the PBL. The orientation of the LLJ was almost in the direction of the rainband. It formed a small angle ($\sim 10°$) relative to the wind-shift line. The rainband traveled at a slow speed of 2.5 m s^{-1} from the north-northwest due to the weak environmental wind (4–5 m s^{-1} from the northwest) in the PBL. The rainband was 5–10 km wide and was composed of many cells. Each cell was accompanied by the moderate convective updraft (6–8 m s^{-1}) and the weak convective downdraft (2–4 m s^{-1}). As the updraft air reached 5 km and higher, it reversed its direction to merge with the northwesterly flow in the middle and upper troposphere (Figs. 21–23). As a result, the reflectivity core was elongated toward the southeast with the environmental shear vector. This elongated reflectivity core induced a convective downdraft on the warm side of the front due largely to precipitation loading (see the convective downdraft CD in Fig. 25). The descending air of this weak convective downdraft produced a horizontally diverging flow in the PBL. Part of this cool diverging

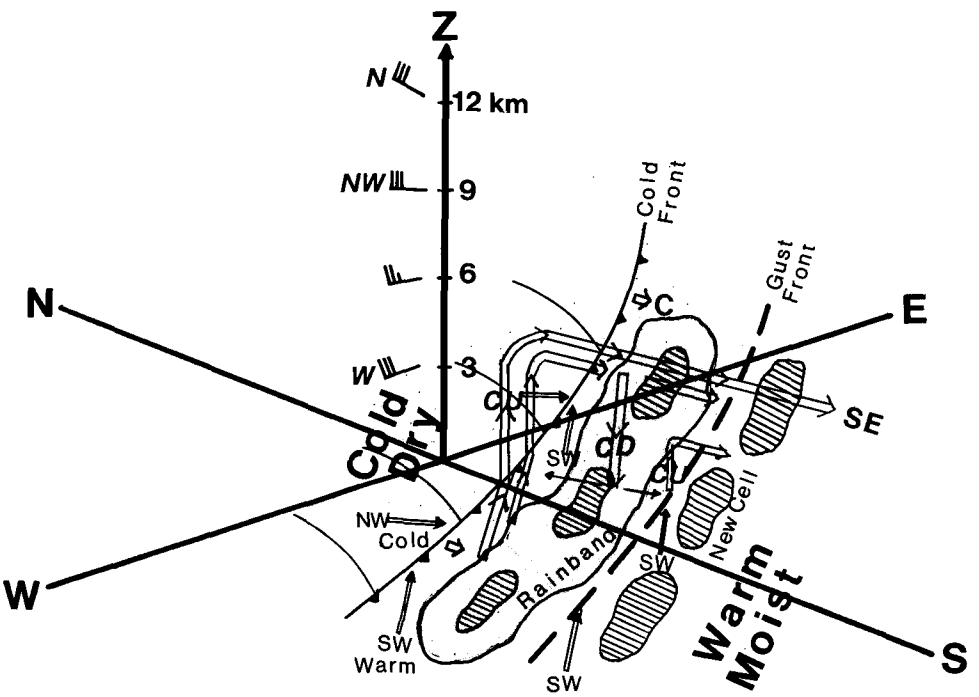

FIG. 25. A schematic diagram showing the development and maintenance of the prefrontal convective rainband during TAMEX IOP 13. The rainband is lightly shaded and the individual cells are hatched. The convective updraft (CU) and downdraft (CD) are indicated. Line motion (C) is from the north-northwest at 2.5 m s^{-1}. The southwest (SW) warm monsoon flow and northwest (NW) cold flow from the mainland of China at low levels are also indicated. An elongation of the reflectivity cores toward the southeast (SE) is in the direction of the environmental shear vector.

flow moved southeastward, interacting with the incoming high-θ_e air to form a gust front (heavy dashed line) in the warm sector. As a result, new cells developed ahead of the gust front, thereby prolonging the life span of the rainband. These new cells moved northeastward at a speed faster than the system speed following the prevailing southwest flow. The precipitation was deep but not intense on the warm side of the front. The maximum reflectivity was less than 42 dBZ. By contrast, the precipitation behind the front was weak and shallow, showing the stratiform precipitation. The area of the stratiform region was narrow due to the dominance of a northwesterly flow in the layers above 5 km.

In summary, the maintenance of this long-lived rainband appears to be caused by the factors of 1) frontal lifting; 2) a gust front arising from the convective downdraft ahead of the front; and 3) discrete developments in advance of the line. These mechanisms are different from those for the squall line in IOP 2 discussed in the study by Wang et al. (1990).

6. Conclusions

The dual-Doppler winds on 25 June 1987 during TAMEX IOP 13 were used to study certain mesoscale structural features of the convective rainband associated with a Mei-Yu front. Only the kinematic structure is presented in Part I, while the dynamic and thermodynamic structures derived from a thermodynamic retrieval method will be presented in Part II.

Results show that 1) the LLJ prevails in the PBL and is oriented in the direction almost parallel to the convective rainband; 2) on the warm side of the convection to the southeast of the front, the precipitation cores in the middle and upper layers are elongated downshear toward the southeast in the direction nearly parallel to the environmental shear vector; 3) weak convective downdrafts form underneath the elongated precipitation cores ahead of the front, producing new cells to the southeast of the gust fronts; 4) the convection is deep and moderate (with maximum updraft speeds less than 10 m s^{-1}) in a broad area ahead of the front and is shallow and weak in the region behind the front; 5) precipitation in the warm sector is widespread but not intense with a maximum reflectivity less than 42 dBZ; and 6) heavy rainfall on the west coast of central Taiwan was mainly caused by the slow movement of the system (2.5 m s^{-1}).

Acknowledgments. The authors with to express their appreciation to those scientists, technicians, and staff members who participated in the TAMEX project. We would like to thank the National Center for Atmospheric Research (NCAR) for providing Doppler data and technical assistance. We are grateful to H. Shen and M. Beeson of Saint Louis University for assistance in data processing. Special thanks go to the National Science Council of the Republic of China and the National Science Foundation of the United States for supporting the field experiment. Discussions with M. LeMone, D. Parsons, and S. Trier of NCAR, Tai-Chi Chen Wang of National Central University, and Ben Jou of National Taiwan University are greatly appreciated. The suggestions by M. LeMone and three anonymous reviewers have contributed to the improvement of the manuscript. This work has been supported by the Atmospheric Science Division, National Science Foundation, under NSF Grant ATM-9012135.

REFERENCES

Browning, K. A., and T. W. Harrold, 1970: Air motion and precipitation growth at a cold front. *Quart. J. Roy. Meteor. Soc.*, **96,** 369–389.

——, and C. W. Pardoe, 1973: Structure of low-level jet streams ahead of mid-latitude cold fronts. *Quart. J. Roy. Meteor. Soc.*, **99,** 619–638.

Carbone, R., 1982: A Severe frontal rainband. Part I: Stormwide hydrodynamic structure. *J. Atmos. Sci.*, **39,** 258–279.

——, 1983: A severe frontal rainband. Part II: Tornado parent vortex circulation. *J. Atmos. Sci.*, **40,** 2639–2654.

Charba, J., 1974: Application of gravity current model to analysis of squall-line gust front. *Mon. Wea. Rev.*, **102,** 140–156.

Chen, Y. L., Y.-X. Zhang, and N. B.-F. Hui, 1989: Analysis of a surface front during the early summer rainy season in Taiwan. *Mon. Wea. Rev.*, **117,** 909–931.

Gal-Chen, T., 1978: A method for the initialization of the anelastic equations. Implications for matching models with observations. *Mon. Wea. Rev.*, **106,** 587–606.

Hobbs, P. V., and O. G. Persson, 1982: The mesoscale and microscale structure and organization of clouds and precipitation in midlatitude cyclones. Part V: The substructure of narrow cold-frontal rainbands. *J. Atmos. Sci.*, **39,** 280–295.

Houze, R. A., Jr., P. V. Hobbs, K. R. Biswas, and W. M. Davis, 1976: Mesoscale rainbands in extratropical cyclones. *Mon. Wea. Rev.*, **104,** 868–878.

Jorgensen, D. P., and M. A. LeMone, 1989: Vertical velocity characteristics of oceanic convection. *J. Atmos. Sci.*, **46,** 621–640.

Jou, B. J., and S. M. Deng, 1990: Mesoscale characteristics of Mei-Yu front: A TAMEX case study. *Proc., Workshop on TAMEX Scientific Results,* Boulder, NCAR, 150–157. [Available from National Center for Atmospheric Research, Boulder, Colorado 80307]

Kuo, Y. H., and G. T. J. Chen, 1990: The Taiwan Area Mesoscale Experiment (TAMEX): An overview. *Bull. Amer. Meteor. Soc.*, **71,** 488–503.

Lemaitre, Y., G. Scialom, and P. Amayenc, 1989: A cold frontal rainband observed during the LANDES-FRONTS 84 Experiment: Mesoscale and small-scale structure inferred from dual-Doppler radar analysis. *J. Atmos. Sci.*, **46,** 2215–2235.

Lin, P. L., T. C. Wang, and C. C. Yeh, 1990: The internal structure of a long-lived rainband revealed from dual-Doppler analysis in TAMEX IOP-13. *Proc., Workshop on TAMEX Scientific Results,* Boulder, NCAR, 26–33. [Available from National Center for Atmospheric Research, Boulder, Colorado 80307]

Lin, Y. J., T. C. Wang, and J. H. Lin, 1986: Pressure and temperature perturbations within a squall-line thunderstorm derived from SESAME dual-Doppler data. *J. Atmos. Sci.*, **43,** 2302–2327.

——, ——, R. W. Pasken, H. Shen, and Z. S. Deng, 1990: Characteristics of a subtropical squall line determined from TAMEX

dual-Doppler data. Part II: Dynamic and thermodynamic structures and momentum budgets. *J. Atmos. Sci.*, **47,** 2382–2399.
——, H. W. Chang, and R. W. Pasken, 1992: The structure of a subtropical prefrontal convective rainband. Part II: Dynamic and thermodynamic structures and momentum budgets. *Mon. Wea. Rev.*, submitted.
Maddox, R. A., 1980: Mesoscale convective complexes. *Bull. Amer. Meteor. Soc.*, **61,** 1374–1387.
Mannouji, N., and K. Kurihara, 1990: A numerical experiment of TAMEX IOP #13 by the spectral limited area model of JMA. *Proc., Workshop on TAMEX Scientific Results,* Boulder, NCAR, 121–126. [Available from National Center for Atmospheric Research, Boulder, Colorado 80307]
Matejka, T. J., R. A. Houze, Jr., and P. V. Hobbs, 1980: Microphysics and dynamics of clouds associated with mesoscale rainbands in extratropical cyclones. *Quart. J. Roy. Meteor. Soc.*, **106,** 29–56.
Parsons, D. B., and S. B. Trier, 1989: Taiwan Area Mesoscale Experiment: Doppler radar operations summary. *NCAR Technical Note,* NCAR/TN-315+STR, 59 pp.
——, C. G. Mohr, and T. Gal-Chen, 1987: A severe frontal rainband. Part III: Derived thermodynamic structure. *J. Atmos. Sci.*, **44,** 1615–1631.
Szoke, E. J., E. J. Zipser, and D. P. Jorgensen, 1986: A radar study of convective cells in mesoscale convective systems in GATE. Part I: Vertical profile statistics and comparison with hurricanes. *J. Atmos. Sci.*, **43,** 182–197.
Trier, S. B., D. B. Parsons, and T. J. Matejka, 1989: Observations of a cold front during TAMEX. *Proc., Workshop on TAMEX Preliminary Scientific Results,* Taipei, Natl. Sci. Council, 186–195. [Available from National Center for Atmospheric Research, Boulder, Colorado 80307]
——, ——, and ——, 1990: Observations of a subtropical cold front in a region of complex terrain. *Mon. Wea. Rev.*, **118,** 2449–2470.
Von Kármán, T., 1940: The engineer grapples with nonlinear problems. *Bull. Amer. Math. Soc.*, **46,** 615–623.
Wang, T. C., Y. J. Lin, R. W. Pasken, and H. Shen, 1990: Characteristics of a subtropical squall line determined from TAMEX dual-Doppler data. Part I: Kinematic structure. *J. Atmos. Sci.*, **47,** 2357–2381.
Wilson, J. W., R. D. Roberts, C. Kessinger, and J. McCarthy, 1984: Microburst wind structure and evaluation of Doppler radar for airport wind shear detection. *J. Climate Appl. Meteor.*, **23,** 898–915.